Award Number: W81XWH-21-1-0728

TITLE: Interrogation of the KDM1A-IL18 Axis in Pediatric High-Grade Glioma

PRINCIPAL INVESTIGATOR: Oren Becher MD

CONTRACTING ORGANIZATION: Icahn School of Medicine at Mount Sinai, New York, NY

REPORT DATE: October 2022

TYPE OF REPORT: Annual

PREPARED FOR: U.S. Army Medical Research and Development Command
Fort Detrick, Maryland 21702-5012

REPORT DOCUMENTATION PAGE

Form Approved
OMB No. 0704-0188

1. REPORT DATE *(DD-MM-YYYY)*	**2. REPORT TYPE**	**3. DATES COVERED** *(From - To)*
October 2022	Annual	30Sep2021-29Sep2022

4. TITLE AND SUBTITLE

Interrogation of the KDM1A-IL18 Axis in Pediatric High-Grade Glioma

5a. CONTRACT NUMBER
W81XWH-21-1-0728

5b. GRANT NUMBER
CA200642

5c. PROGRAM ELEMENT NUMBER

6. AUTHOR(S)

Oren Becher MD

5d. PROJECT NUMBER

5e. TASK NUMBER

5f. WORK UNIT NUMBER

7. PERFORMING ORGANIZATION NAME(S) AND ADDRESS(ES)

ICHAN SCHOOL OF MEDICINE
AT MOUNT SINAI
ONE GUSTAVE L LEVY PL
NEW YORK NY 10029-6504

8. PERFORMING ORGANIZATION REPORT NUMBER

9. SPONSORING / MONITORING AGENCY NAME(S) AND ADDRESS(ES)

U.S. Army Medical Research and Development Command
Fort Detrick, Maryland 21702-5012

10. SPONSOR/MONITOR'S ACRONYM(S)

11. SPONSOR/MONITOR'S REPORT NUMBER(S)

12. DISTRIBUTION / AVAILABILITY STATEMENT

Approved for Public Release; Distribution Unlimited

13. SUPPLEMENTARY NOTES

14. ABSTRACT

Diffuse Intrinsic Pontine Glioma (DIPG) is a type of high-grade glioma that remains uniformly fatal in 2022, represents the leading cause of death for pediatric brain tumor patients, and for which the standard of care has not improved in over 50 years. In addition, despite at least 100 clinical trials, there is not a single drug that has been shown to significantly prolong the survival of children with DIPG beyond radiation alone.The objective of our study is to unravel the role of LSD1 or KDM1A in DIPG pathogenesis focusing on its effect on immune related genes. We hypothesize that LSD1 promotes gliomagenesis in part by repressing immune-related genes such as IL18, and that inhibition of KDM1A will be efficacious in prolonging the survival of DIPG-bearing mice, in part through upregulation of IL18, thereby altering the tumor microenvironment. At the end of year 1, we have made progress toward accomplishing the Statement of Work and our data suggests that LSD1 is a bone-fide therapeutic target in DIPG. In the upcoming two years we will clarify the mechanism and prioritize a drug and potentially a combination therapy for clinical translation.

15. SUBJECT TERMS
Diffuse Intrinsic Pontine Glioma, LSD1, pediatric brain cancer

16. SECURITY CLASSIFICATION OF:			**17. LIMITATION OF ABSTRACT**	**18. NUMBER OF PAGES**	**19a. NAME OF RESPONSIBLE PERSON**
a. REPORT	**b. ABSTRACT**	**c. THIS PAGE**			USAMRDC
Unclassified	Unclassified	Unclassified	Unclassified	36	**19b. TELEPHONE NUMBER** *(include area code)*

TABLE OF CONTENTS

1. **INTRODUCTION:**

Diffuse Intrinsic Pontine Glioma (DIPG) is a type of high-grade glioma that remains uniformly fatal in 2020, represents the leading cause of death for pediatric brain tumor patients, and for which the standard of care has not improved in over 50 years. In addition, despite at least 100 clinical trials, there is not a single drug that has been shown to significantly prolong the survival of children with DIPG beyond radiation alone.The objective of our study is to unravel the role of LSD1 or KDM1A in DIPG pathogenesis focusing on its effect on immune related genes. We hypothesize that LSD1 promotes gliomagenesis in part by repressing immune-related genes such as IL18, and that inhibition of KDM1A will be efficacious in prolonging the survival of DIPG-bearing mice, in part through upregulation of IL18, thereby altering the tumor microenvironment.

2. **KEYWORDS:**
3. **ACCOMPLISHMENTS:**

- **What were the major goals of the project?**

- **Specific Aim 1**: Determine the effects of LSD1 deletion and overexpression in DIPG pathogenesis in vivo in genetic and xenograft models
- **Specific Aim 2 -**Determine whether IL18 is a direct target gene of LSD1 and elucidate the function of IL18 in DIPG pathogenesis using both genetic and xenograft models of DIPG
- **Specific Aim 3** Determine the efficacy of LSD1 inhibitors in genetic and xenograft models of DIPG.

- **What was accomplished under these goals?**

- With regards to aim 1, we have assessed the effect of LSD1 overexpression on tumorigenesis- part of **Subtask 2.1**, **Subtask 3.1**, and **Subtask 3.2**. We overexpressed WT LSD1, a truncation LSD1 mutant lacking the demethylase domain, and empty vector in our DIPG model. Interestingly, our preliminary data suggests that the truncation mutant may slow down tumorigenesis, perhaps by acting as a dominant negative. This is illustrated in figure 1 and 2. In brief, neonatal pups were infected with the following vectors to induce tumor formation and mice were monitored closely for signs and symptoms of brain tumor formation. All the experimental groups included the following 3 vectors: RCAS-PDGFB, RCAS-H3.3K27M, and RCAS-CRE to delete p53. The variable vectors between the cohorts were WT LSD1, Mutant LSD1 (truncation mutant without the C-terminus demethylase domain) and empty vector. Additional details regarding our genetic mouse modeling approach are in the appendix (a published reference[1].

We have made progress towards aims 2 (**preparatory studies for subtask 1**) and 3 (**subtask 1**) in terms of examining IL-18 expression and determining the efficacy of LSD1 inhibitors in patient derived

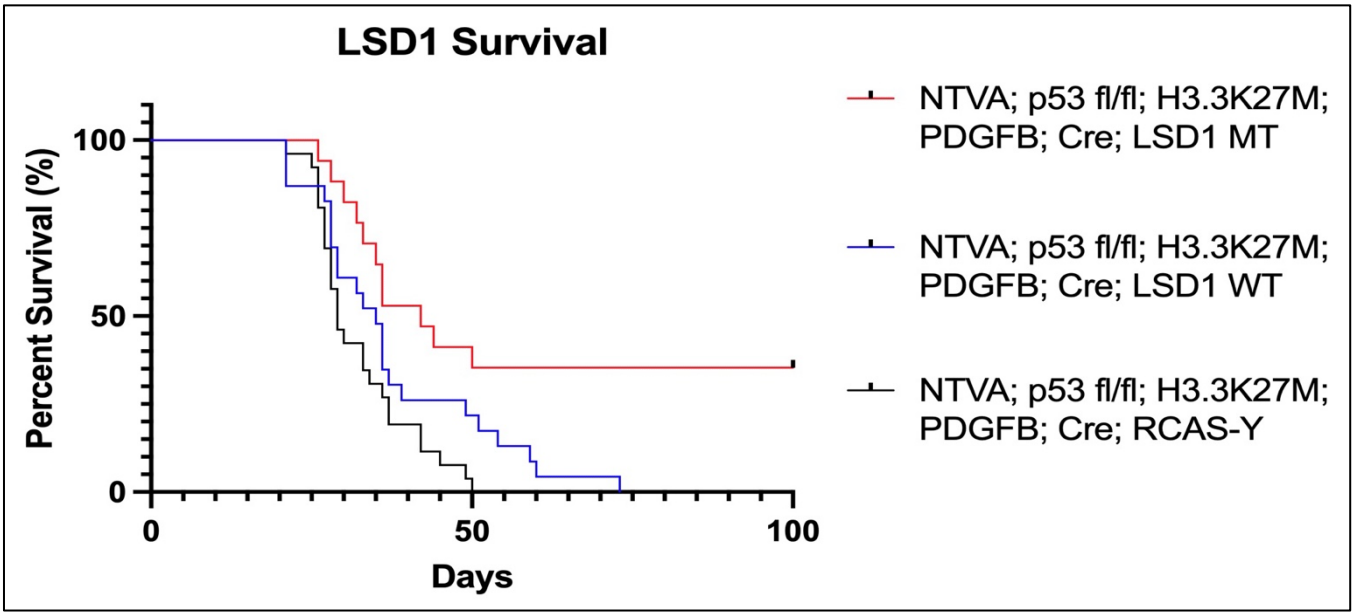

Figure 1. survival curve of murine DIPG initiated with PDGFB; H3.3K27M; and p53 loss

Comparison of the effects of LSD1 WT overexpression, LSD1 truncation mutant (MT), to empty vector, or (RCAS-Y). Preliminary data suggests that LSD1 MT significantly delay tumor formation. The following comparisons were made by the log-rank test: LSD1 WT vs. LSD1 MT; p<0.0148* LSD1 WT vs. RCAS-Y; p<0.0629 ns. LSD1 MT vs. RCAS-Y; p<0.0010***

models of DIPG**.** We have carried out experiments to test pharmacological inhibition with clinically relevant LSD1 inhibitors in a series of DIPG cells lines. In Figure 3 we evaluated cell v viability after DIPG cells were subject to either 120 hours or 96 hours of drug exposure. AlamarBlue cell viability assay was completed and read with the CLARIOstar® plus microplate reader. Data is reported as relative fluorescent units (RFU) and is shown as mean ± standard deviation. The IC_{50} was determined on Prism9 using a nonlinear regression analysis with [inhibitor] vs. normalized response to fit the dose response curve to a variable slope. These results indicate that IMG-7289 has the lowest IC50 of any of the inhibitors tested.

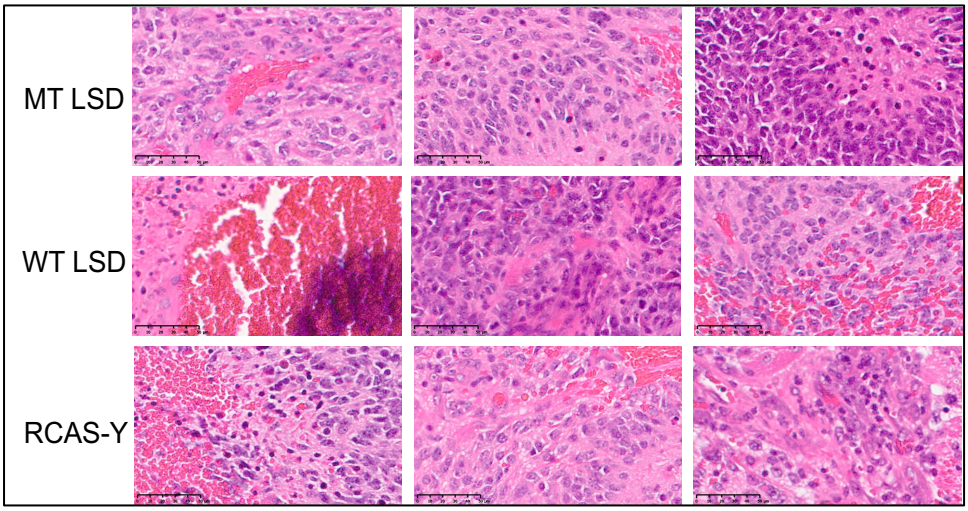

Figure 2. Representative high magnification (40X) H&Es of the cohorts in Figure 1

Preliminary analysis Suggests that there is not a significant difference in tumor grade across tumors. As expected, tumors had high grade histology.

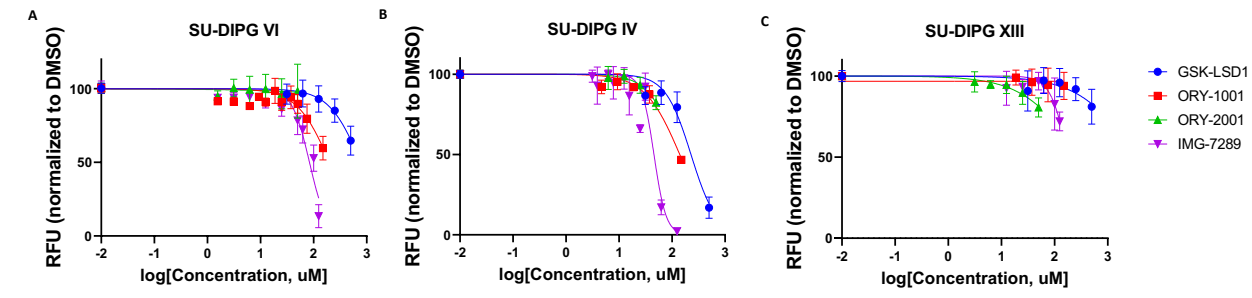

D

	IC_{50} (uM)			
	GSK-LSD1	ORY-2001	IMG-7289	ORY-1001
SU-DIPG XII	> 500	> 50	179.2	> 150
SU-DIPG VI	> 500	> 50	83.67	> 150
SU-DIPG IV	227.7	> 50	45.62	140.0

Figure 3. Single Agent Activity of LSD1 inhibition in a SU-DIPG models. A) SU-DIPG VI, **B)** SU-DIPG IV, **C)** SU-DIPG XIII lines were treated for with either GSK-LSD1, ORY-1001, ORY-2001, or IMG-7289 and measured using an AlamarBlue cell viability assay. **D)** Table summarizing the IC50 values for each LSD1 inhibitor among the various cell lines.

Pharmacological inhibition of LSD1 in HGG is promising, but optimization of the treatment regimens will be necessary to sustain antitumor responses. In liquid cancer models, mitogen-activated protein kinase (**MAPK**) signaling activation acts as a mechanism of resistance to LSD1 inhibitors. This pathway is relevant in GBM and DIPG because it is frequently hyperactivated, in part via mutations and/or amplification of receptor tyrosine kinases (**RTKs**). Western blot analyses were carried out in DIPG cell lines treated with LSD1 inhibitors for 120 hours (SU-DIPG XIII and SU-DIPG VI) or 72 hours (SU-DIPG IV). After LSD1 inhibitor treatment, cells were harvested, and protein lysates were made using RIPA buffer. Protein concentration was quantified with the Bradford assay and equal amounts (50 ug XIII, 60 ug VI, and 30 ug IV) were loaded onto an 8% (XIII) or 10% (VI and IV) polyacrylamide gel for Western blot analysis. Images were developed with ECL reagent using a ChemiDoc™ Touch Imaging System. Data shown below in Fig 4 indicates activation of ERK and AKT

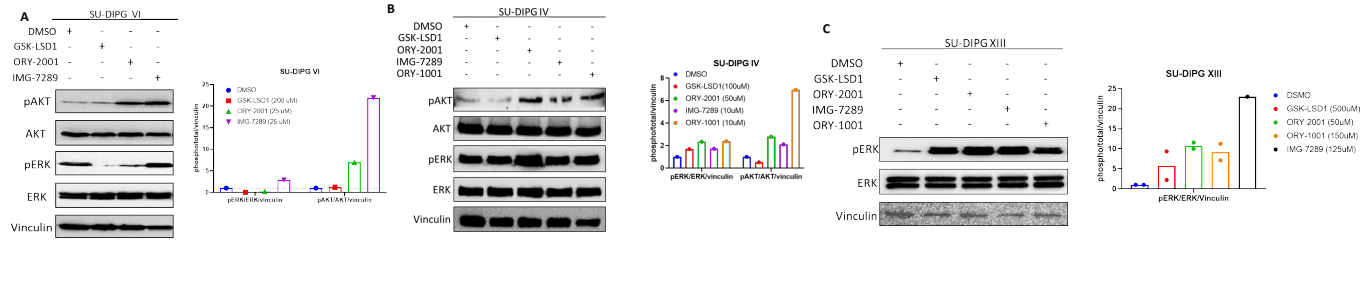

Figure 4. Activation of kinase signaling after LSD1 inhibition. A) SU-DIPG VI **B)** SU-DIPG IV, and **C)** SU-DIPG XIII cell lines underwent 120h – SU-DIPG XIII and SU-DIPG VI – or 72 hours – SU-DIPG IV – of treatment with either GSK-LSD1, ORY-1001, ORY-2001, or IMG-7289. Cells were then harvested and lysate for western blot analysis. The blots were then probed for phosphorylated ERK and AKT while normalized to total protein and vinculin as a loading control.

signaling. Based on these results we will test if enhancing efficacy of LSD1 inhibition through kinase inhibitor combination is a rational strategy.

Relevant to aim 2, we have tested pharmacological inhibition of LSD1 on transcript and protein levels of IL-18. Figure 4 shows quantitative PCR of IL-18 transcript in DIPG IV cells. Although an increase in IL-18

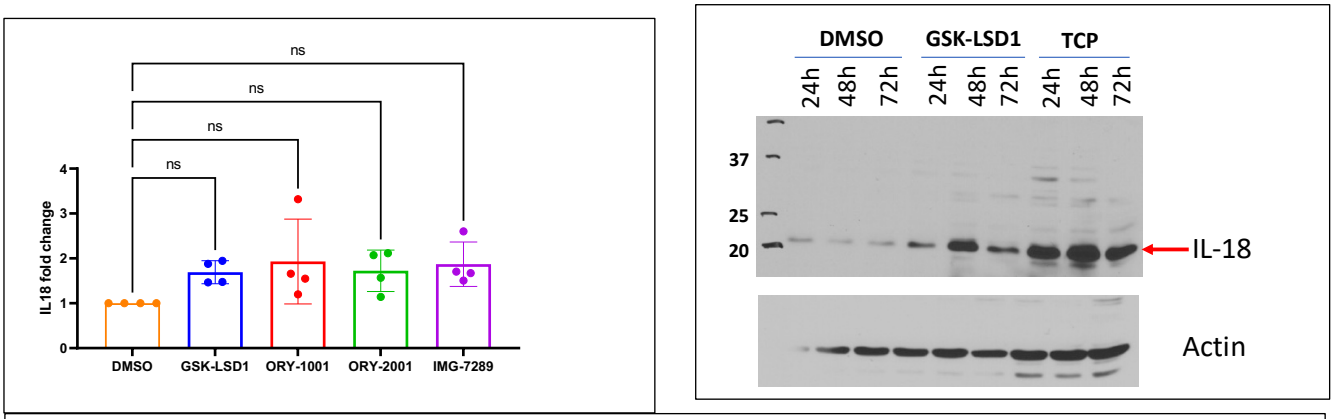

Figure 5. IL-18 transcript and protein expression in high grade glioma cell lines after exposure to LSD1 inhibitors.

transcript is apparent after 24 h of exposure with the indicated doses, the increase does not reach statistical significance. However, protein expression of IL-18 as measured by western blotting appears elevated as shown in Figure 5. Additional experimental details regarding the human DIPG models and some of the in vitro experiments described in the progress report can be found in our initial collaborative paper[2].

- **What opportunities for training and professional development has the project provided?**

  Funds were utilized to support laboratory personnel who had no prior experience with primary patient derived brain tumor cell lines. This enhanced their skill and prompted them to attend seminars relevant to brain tumor therapeutics. A summer student was also trained through funds available for this project.

- **How were the results disseminated to communities of interest?**

  An abstract will be presented at the 2022 Society for Neuro-oncology Conference describing this work. This will be presented as a poster. The title of the abstract is Co-inhibition of kinase signaling pathways and epigenetic regulators overcomes compensatory effects in pediatric high-grade glioma. The presenting author is Jack Adams (Summer student).

- **What do you plan to do during the next reporting period to accomplish the goals?**

  - *We have obtained LSD1 floxed mice and are crossing them into the Ntva mice. We hope to complete the LSD1 deletion experiments by the end of year 2- compare tumorigenesis with and without deletion of LSD1 and subsequent analysis as stated in SOW. In addition, we have generated an RCAS-IL-18, and so will begin the proposed IL18 over-expression experiments in year 2 as stated in SOW.* The in vivo experiments and ChIP experiments will be prioritized in the next year. We will also begin generating knockdown and knockout lines.

4. **IMPACT:**

- **What was the impact on the development of the principal discipline(s) of the project?**

- The project seeks to evaluate whether LSD1 is good therapeutic target to treat this incurable brain cancer. Results in this first year of the award are still supportive of our hypothesis, which is that LSD1 is a good therapeutic target. In year 2 we will continue to evaluate this target and determine how it contributes to tumor formation. Some of the results in year 1 may also suggest a future combination therapy (LSD1 inhibitor + a kinase inhibitor) to explore therapeutically.
- **What was the impact on other disciplines?**
  - *Nothing to Report*
- **What was the impact on technology transfer?**
  - *Nothing to Report*
- **What was the impact on society beyond science and technology?**
  - *Nothing to Report*
  - *I think figuring out how to cure this childhood brain cancer will be of benefit to society. An incurable cancer in children where the standard of care has not budged, has a negative impact on society and particularly the families directly affected by it.*

5. **CHANGES/PROBLEMS:**
   - **Changes in approach and reasons for change**
     - *Nothing to report*
   - **Actual or anticipated problems or delays and actions or plans to resolve them**
     - *Nothing to report*
   - **Changes that had a significant impact on expenditures**
     - *Nothing to report*
   - **Significant changes in use or care of human subjects, vertebrate animals, biohazards, and/or select agents**
     - *Nothing to report. Institutional Review Board/Institutional Animal Care and Use Committee approval dates were 1/13/22 and 4/26/22 respectively.*
   - **Significant changes in use or care of human subjects**
     - No significant changes
   - **Significant changes in use or care of vertebrate animals.**
     - No significant changes
   - **Significant changes in use of biohazards and/or select agents**
     - No significant changes
6. **PRODUCTS:**
   - **Publications, conference papers, and presentations**
     - **Journal publications.** *Nothing to report*

- **Books or other non-periodical, one-time publications.** *Nothing to report.*
- **Other publications, conference papers, and presentations.**

  Poster presentation at the annual Society of Neuro-Oncology meeting. Presenter is Jack Adams. Title of poster is: Co-inhibition of kinase signaling pathways and epigenetic regulators overcomes compensatory effects in pediatric high-grade gliomas.

- **Website(s) or other Internet site(s)**
  Nothing to report
- **Technologies or techniques**
  Nothing to report
- **Inventions, patent applications, and/or licenses**
  nothing to report
- **Other Products**
  Identify any other reportable outcomes that were developed under this project. Reportable outcomes are defined as a research result that is or relates to a product, scientific advance, or research tool that makes a meaningful contribution toward the understanding, prevention, diagnosis, prognosis, treatment, and/or rehabilitation of a disease, injury or condition, or to improve the quality of life. Examples include:
  - RCAS-IL18 – a plasmid that will overexpress murine IL18 in TVA positive cells.

7. **PARTICIPANTS & OTHER COLLABORATING ORGANIZATIONS**
   - **What individuals have worked on the project?**

Name:	Oren Becher
Project Role:	*Principal Investigator*
Researcher Identifier (e.g. ORCID ID):	ORCID ID: 0000-0003-4016-8492
Nearest person month worked:	2.4
Contribution to Project:	Dr. Becher is overseeing the project.
Funding Support:	

Name:	Anna Racanelli, BA
Project Role:	Helping with tumor induction and mouse monitoring
Researcher Identifier (e.g. ORCID ID):	
Nearest person month worked:	3
Contribution to Project:	Technical support. Master's student
Funding Support:	

Name:	Mili Chizhik, BA

Project Role:	Research technician
Researcher Identifier (e.g. ORCID ID):	
Nearest person month worked:	2.4
Contribution to Project:	Technical support: cell culture, tumor induction, and mouse monitoring
Funding Support:	Becher Seed funds

Name:	Joya Chandra
Project Role:	Subcontract PI
Researcher Identifier (e.g. ORCID ID):	ORCID ID: 0000-0003-4016-8492
Nearest person month worked:	2.4
Contribution to Project:	Dr. Chandra is overseeing the project
Funding Support:	

Name:	Huaxian Ma, MS
Project Role:	Research scientist
Researcher Identifier (e.g. ORCID ID):	
Nearest person month worked:	9
Contribution to Project:	Huaxian performed experiments under Dr. Chandra's mentorship
Funding Support:	

Name:	Samantha Gadd, PhD
Project Role:	*Bioinformatics*
Researcher Identifier (e.g. ORCID ID):	ORCID ID:
Nearest person month worked:	1.2
Contribution to Project:	Performing bioinformatics analysis

Funding Support:	

- **Has there been a change in the active other support of the PD/PI(s) or senior/key personnel since the last reporting period?**

  - Dr. Becher has been awarded a new MPI R01 award (6/1/22-5/31/27). Contact PI is Dolores Hambardzumyan. R01 CA258636-01A1 titled: The role of Myeloid cells in pediatric high-grade gliomas. There is no overlap with this award. His effort is 20%.
  - His R01 R01 CA197313-08 has completed and we have submitted a NCE for an additional year. This NCE is still being process by NIH. The period of NCE is 9/1/22-8/31/23. The requested effort for the NCE period is 9%.

- **What other organizations were involved as partners?**

  - **Organization Name:** MD Anderson
  - **Location of Organization:** *Houston TX*
  - **Partner's contribution to the projec**t

    1. **Collaboration** – *This award is a collaboration between Mount Sinai (Oren Becher) and MD Anderson (Joya Chandra) as in the award documents.*

  - **Organization Name:** Ann & Robert H. Lurie Children's Hospital of Chicago
  - **Location of Organization: Chicago, IL**
  - **Partner's contribution to the project**
    1. **Collaboration** – *Sam Gadd, PhD is providing bioinformatics expertise.*

Conclusion-

We have made great progress in year 1 and are excited for year 2: the LSD1 deletion experiment, the IL18 overexpression experiments, additional pharmacological experiments such as BBB penetration with the LSD1 inhibitors to prioritize the one that we will test in vivo in year 3. In year 1 we obtained some key reagents such as the LSD1 floxed mice, generation of the RCAS-IL18 as well as obtaining all the administrative approvals. We did still generate some data that is of interest and is supportive of our original hypothesis that LSD1 inhibitors may be therapeutic to treat DIPG (an incurable brain cancer in children).

References

1. Cordero, F.J., et al., *Histone H3.3K27M Represses p16 to Accelerate Gliomagenesis in a Murine Model of DIPG.* Mol Cancer Res, 2017. **15**(9): p. 1243-1254.
2. Bailey, C.P., et al., *Pharmacologic inhibition of lysine-specific demethylase 1 as a therapeutic and immune-sensitization strategy in pediatric high-grade glioma.* Neuro Oncol, 2020. **22**(9): p. 1302-1314.

Molecular Cancer Research

Histone H3.3K27M Represses *p16* to Accelerate Gliomagenesis in a Murine Model of DIPG

Francisco J. Cordero[1,2], Zhiqing Huang[3], Carole Grenier[3], Xingyao He[4], Guo Hu[1], Roger E. McLendon[2], Susan K. Murphy[3], Rintaro Hashizume[4,5], and Oren J. Becher[1,2,6,7,8,9]

Abstract

Diffuse intrinsic pontine glioma (DIPG) is a highly aggressive pediatric brainstem tumor genetically distinguished from adult GBM by the high prevalence of the K27M mutation in the histone H3 variant H3.3 (*H3F3A*). This mutation reprograms the H3K27me3 epigenetic landscape of DIPG by inhibiting the H3K27-specific histone methyltransferase EZH2. This globally reduces H3K27me2/3, critical repressive marks responsible for cell fate decisions, and also causes focal gain of H3K27me3 throughout the epigenome. To date, the tumor-driving effects of H3.3K27M remain largely unknown. Here, it is demonstrated that H3.3K27M cooperates with PDGF-B *in vivo*, enhancing gliomagenesis and reducing survival of p53 wild-type (WT) and knockout murine models of DIPG. H3.3K27M expression drives increased proliferation of tumor-derived murine neurospheres, suggesting that cell-cycle deregulation contributes to increased malignancy in mutant tumors. RNA sequencing on tumor tissue from H3.3K27M-expressing mice indicated global upregulation of PRC2 target genes, and a subset of newly repressed genes enriched in regulators of development and cell proliferation. Strikingly, H3.3K27M induced targeted repression of the p16/ink4a (*CDKN2A*) locus, a critical regulator of the G_0–G_1 to S-phase transition. Increased levels of H3K27me3 were observed at the p16 promoter; however, pharmacologic reduction of methylation at this promoter did not rescue p16 expression. Although DNA methylation is also present at this promoter, it is not K27M dependent. Intriguingly, inhibition of DNA methylation restores p16 levels and is cytotoxic against murine tumor cells. Importantly, these data reveal that H3.3K27M-mediated p16 repression is an important mechanism underlying the proliferation of H3.3K27M tumor cells, as *in vivo cdkn2a* knockout eliminates the survival difference between H3.3K27M and H3.3WT tumor-bearing mice.

Implications: This study shows that H3.3K27M mutation and PDGF signaling act in concert to accelerate gliomagenesis in a genetic mouse model and identifies repression of p16 tumor suppressor as a target of H3.3K27M, highlighting the G_1–S cell-cycle transition as a promising therapeutic avenue. *Mol Cancer Res; 15(9); 1243–54. ©2017 AACR.*

Introduction

Despite over half a century of research directed toward the development of an efficacious treatment for diffuse intrinsic pontine glioma (DIPG), a rare and deadly tumor arising within the pons region of the brainstem predominantly in children, no therapies have improved the dismal survival rates. DIPG patients have a median survival of less than one year after diagnosis, and less than 20% of patients survive past 2 years. The diffuse and infiltrating nature of the tumor coupled with its extremely sensitive location precludes surgical resection. Currently, the standard regimen of radiotherapy provides only temporary relief from symptoms, and no chemotherapy has shown efficacy beyond radiation alone (1, 2).

Recent large-scale analyses of DIPG patient samples has allowed for major advances in our understanding of the driving mechanisms underlying DIPG. These studies have identified the most commonly occurring genetic alterations, which include H3.3/H3.1 K27M mutations (80%), mutations in *TP53* (77%), and amplification of *PDGFRA* (36%; refs. 3–11). The H3 histone mutations not only differentiate pediatric from adult gliomas, but also define distinct gene expression profiles between cortical and brainstem gliomas specific to the particular amino acid tail residue mutations (12). The H3.3K27M mutation has increasingly gained interest due to its high frequency, specific spatiotemporal occurrence, and gain-of-function mechanism of action. H3.3K27M histones act as potent inhibitors of H3K27 di- and trimethylation (H3K27me2/3) by binding to the SET domain of EZH2, the histone methyltransferase component of the Polycomb repressive complex 2 (PRC2) causing global reduction of these repressive marks (13). The H3.3K27M-mediated global changes

[1]Division of Hematology-Oncology, Department of Pediatrics, Duke University Medical Center, Durham, North Carolina. [2]Department of Pathology, Duke University Medical Center, Durham, North Carolina. [3]Division of Gynecologic Oncology, Department of Obstetrics and Gynecology, Duke University Medical Center. [4]Department of Molecular Genetics, Northwestern University Feinberg School of Medicine, Chicago, Illinois. [5]Department of Neurological Surgery, Northwestern University Feinberg School of Medicine, Chicago, Illinois. [6]Department of Pharmacology and Cancer Biology, Duke University Medical Center, Durham, North Carolina. [7]Preston Robert Tisch Brain Tumor Center, Duke University Medical Center, Durham, North Carolina. [8]Department of Pediatrics, Northwestern University Feinberg School of Medicine, Chicago, Illinois. [9]Ann & Robert Lurie Children's Hospital of Chicago, Chicago, Illinois.

Note: Supplementary data for this article are available at Molecular Cancer Research Online (http://mcr.aacrjournals.org/).

Corresponding Author: Oren J. Becher, Department of Pediatrics, Northwestern University, 320 East Superior Street, Searle 13-560, Chicago, IL 60611. Phone: 312-503-6562; Fax: 312-227-9756; E-mail: oren.becher@northwestern.edu

doi: 10.1158/1541-7786.MCR-16-0389

comprise a specific epigenetic signature that may hold valuable insight into the driving mechanisms behind this aggressive disease (14, 15).

Chromatin immunoprecipitation sequencing (ChIP-seq) and whole-genome bisulfite sequencing studies of K27M-mutant DIPG and pediatric high-grade glioma patient samples identified focal regions retain or gain H3K27me3 along with the global loss of H3K27me3 and subsequent DNA hypomethylation profile (15). The *CDKN2A* locus was included as a site of novel PRC2-dependent gain of promoter H3K27me3 (14). Homozygous deletion of the *CDKN2A* locus, which harbors both the p16/*INK4A* and p19/*ARF* transcripts, although a common genetic alteration across all human cancer types, rarely occurs in DIPG (16). Although the tumor suppressor function of p16, an endogenous CDK4/6 inhibitor, has been thought to remain predominantly uncompromised in DIPG, phase I clinical trials are under way assessing the safety of CDK4/6 inhibitors in treating affected children (17). To date, however, no work has demonstrated whether this novel increase in H3K27me3 at the *CDKN2A* locus is directly mediated by the H3.3K27M oncohistone to regulate its expression or whether repression of this locus contributes to gliomagenesis.

To address the role of H3.3K27M in DIPG, we developed an *in vivo* brainstem glioma mouse model incorporating the H3.3K27M mutation and platelet-derived growth factor-B (PDGFB) activation, in both p53 wild-type (WT) and knockout settings, using the RCAS/tv-a avian retroviral system (13, 18). We demonstrate that the expression of H3.3K27M cooperates with PDGF signaling to increase proliferation and tumor grade *in vivo* in both p53 WT and deficient models. Intriguingly, H3.3K27M causes global gene derepression as expected, but also novel gene repression. We find that p16 is a target for aberrant H3.3K27M-induced repression and although there is a localized gain in promoter H3K27me3, only inhibition of DNA methylation rescues gene expression. Importantly, genetic knockout of *cdkn2a* abolishes the survival difference between mice harboring H3.3K27M- and H3.3WT-expressing tumors. In addition, H3.3K27M-expressing tumor cells show significantly increased sensitivity to CDK4/6 inhibition by palbociclib compared with H3.3WT controls. This establishes the H3.3K27M-induced repression of p16 as a critical mechanism contributing to the acceleration of gliomagenesis by the mutation and highlights regulation of the G_1–S transition as a promising therapeutic node in DIPG.

Materials and Methods

In vivo mouse model experiments

All animals were maintained in accordance with the Duke Animal Care and Use Committee under the approved protocol (A162-16-07). The following mice were used: Nestin Tv-a; $p53^{fl/fl}$ (C57BL/6J background) as described previously (19). Nestin Tv-a; $CDKN2A^{fl/fl}$ mice (C57BL/6J background) were obtained by crossing nestin tv-a mice with $cdkn2a^{fl/fl}$ mice, provided by Ron Depinho (University of Texas MD Anderson Cancer Center, Houston, TX). Mice were monitored for tumor growth by weight loss and neurologic symptoms.

Cell lines and culture

Murine tumors were isolated and enzymatically digested as described previously (19). GFP-positive single cells were sorted by FACS and cultured in NeuroCult media with proliferation supplement (Stemcell Technologies) as neurospheres. Cells were split using Accutase (Innovative Cell Technologies), and all experiments were performed using primary (non-thawed) lines at low passage (under passage 10). For bromodeoxyuridine (BrdUrd) analysis, single cells were seeded into 96-well plates in biological and experimental triplicate, cultured for 72 hours, and then assessed for BrdUrd incorporation using the Cell Proliferation ELISA Kit (Roche) per the manufacturer's recommendations. For drug treatments of both murine and human DIPG lines, single cells were seeded into 96-well plates in biological and experimental triplicate and treated with drugs or vehicle (0.1% DMSO) the following day. Primary pediatric human glioma cell lines, SF8628 and DIPG007 (HSJD-DIPG-007), contain H3.3K27M mutations, SU-DIPG-IV contains H3.1K27M, and all lines were obtained from Dr. Rintaro Hashizume at Northwestern University (Chicago, IL), Dr. Michelle Monje at Stanford University (Stanford, CA), and Dr. Angel Montero Carcaboso at Hospital Sant Joan de Déu (Barcelona, Spain), in accord with institutionally approved protocol at each institution, and the cell culture models have been described previously (20–22). SF8628 cells derived from surgical biopsy were maintained as an exponentially growing monolayer in complete medium consisting of DMEM (GIBCO 11965, Invitrogen) supplemented with 10% FBS with penicillin–streptomycin and plasmocin. SU-DIPG IV cell culture derived from DIPG autopsy tissue was grown as tumor neurospheres in tumor stem media (TSM) consisting of DMEM/F12 (Invitrogen), Neurobasal(-A) (Invitrogen), B27(-A) (Invitrogen), human-bFGF (20 ng/mL; Shenandoah Biotechnology), human-EGF (20 ng/mL; Shenandoah Biotechnology), human PDGF-AB (20 ng/mL; Shenandoah Biotechnology), and heparin (10 ng/mL). DIPG007 (HSJD-DIPG-007) cells were derived from the autopsy and were maintained as an exponentially growing monolayer in TSM media supplemented with 5% FBS. Human cell histone mutational status was determined using Sanger sequencing for the *H3F3A* and *HIST1H3B* genes. Human cell cultures were validated by DNA fingerprinting using short tandem repeat analysis and checked for mycoplasma contamination. Human lines were cultured for 2 to 3 passages (2 weeks) following thawing for experiments. Other experimental details are as described in the text. Inhibitors used were GSK343, GSK126, EPZ-6438, decitabine, azacitidine, and palbociclib (Selleck). No mycoplasma testing regimen was performed on murine cell lines as they are early passage tumor-derived cells.

Generation of murine brainstem gliomas

All animal studies were performed in accordance with the Duke University Animal Care and Use Committee and Guide for the Care and Use of Laboratory Animals (protocol # A214-13-08). The RCAS/TVA system was used to generate murine brainstem gliomas. DF1 virus–producing cells were purchased from ATCC, cultured in DMEM (ATCC) supplemented with 10% FBS, 2 mmol/L L-glutamine, 100 U/mL penicillin and 100 μg/mL streptomycin, and incubated at 39°C and 5% CO_2. Cells were transfected with RCAS plasmids (RCAS-PDGF-B, RCAS-Cre, RCAS-H3.3WT, RCAS-H3.3K27M, RCAS-p53shRNA) using X-TremeGENE 9 (Roche) per the manufacturer's instructions. One microliter (10^5 cells) of DF1 cells (ATCC) expressing equal ratios of RCAS virus–producing cells was injected intracranially into the brainstem of postnatal day 3 to 4 nestin tv-a (Ntv-a) $p53^{fl/fl}$ mice to generate brainstem gliomas as described previously (19). Mice

were euthanized with CO_2 upon appearance of symptoms of brain tumor development (weight loss, lethargy, head tilt, or hydrocephalus) in accordance with Duke University IACUC protocol. Brain tissue from these animals was extracted and either fixed in 10% neutral-buffered formalin and paraffin embedded or used to generate tumor cell lines.

In vitro infection of brainstem progenitors with RCAS viruses

Normal brainstem progenitors from nestin-tv-a mice were isolated and infected with concentrated RCAS-H3.3K27M-HA, RCAS-H3.3WT-HA, or RCASY (empty vector) viruses as previously described and grown under neurosphere conditions (23).

Tumor grading

Tumor samples fixed in 10% formalin for 24 hours were embedded in paraffin by the Duke Pathology Core and cut into 5-μm sections using a Leica RM2235 microtome. Hematoxylin and eosin (H&E) staining was performed using standard protocols. Tumor grading was performed by a blinded neuropathologist (R.E. McLendon).

IHC analysis

Formalin-fixed brains were paraffin embedded by Duke Pathology Core Services. Sections were cut 5-μm thick using a Leica RM2235 Microtome. IHC was performed using an automated processor (Discovery XT, Ventana Medical Systems, Inc.). Antibodies used are provided in the Supplementary Material. Quantification was performed using Metamorph software. We analyzed 10 different high-powered fields (40×) and quantified total nuclear area of positive staining to total nuclear area.

Immunofluorescence studies

Tumor-bearing mice were injected with EdU (10 mg/kg) 4 hours prior to sacrifice; brains were fixed in 10% formalin, paraffin embedded, and cut into 5-μm sections. Slides were deparaffinized in xylenes and rehydrated with decreasing ethanol solutions. EdU staining was performed following the protocol for Click-iT EdU Alexa Fluor 594 Imaging Kit (Invitrogen #C10339). Quantification was performed using Metamorph software. We analyzed 10 different high-powered fields (40×) and quantified total EdU-positive staining to total nuclear area (DAPI stained).

Western blots

Western blots on histone-extracted proteins were performed as described previously (13). Antibodies used are provided in the Supplementary Material. Quantification of band intensities was performed using ImageJ software.

MRI tumor volume analysis

T2-weighted scans of the brain were acquired using a cryogenic coil (CryoProbe, Bruker Biospin) and the following parameters: repetition time TR = 1.5 seconds, echo time TE = 22 ms, bandwidth 75 kHz, flip angle 90, matrix: 160 × 160, 100 slices, field of view 1.6 × 1.6 × 1.0 cm. Tumor volumes were obtained from manual segmentation.

RNA-seq analysis

Read-pairs were aligned to the mouse genome (mm9) by expression analysis. The number of read-pairs per gene was determined based upon the NCBIM37 gene annotation from the ENSEMBL database (24). Genes that did not have at least 10 read-pairs in any single library were excluded from further analysis. Normalization and differential expression analysis was carried out using the DESeq bioconductor package (default parameters, GSE98765; ref. 25).

qRT-PCR analysis

Total RNA was isolated using RNeasy kit (Qiagen) per the manufacturer's protocol. cDNA was synthesized from total mRNA using Superscript II and OligodT primers (Invitrogen). qRT-PCR TaqMan primers were used for murine p16, and murine p19 and sequences are provided in the Supplementary Material. Relative gene expression levels were generated using the $\Delta\Delta C_t$ method (26).

Flow cytometry

Cell-cycle analysis by flow cytometry was performed by fixing cells in 70% ethanol on ice for 15 minutes. Cells were washed, stained with propidium iodide labeling solution (BD Biosciences), and transferred to FACS tubes. Cell-cycle analysis was performed by the Duke Cancer Center Flow Cytometry Core.

ChIP followed by quantitative PCR

Tumor neurospheres were dissociated using Accutase (Innovative Cell Technologies) and counted using the Scepter automated cell counter (Millipore). Cells (5×10^6) were fixed in 1% formaldehyde for 7 minutes at room temperature, quenched with the addition of 125 mmol/L glycine for 5 minutes, and washed with 1× PBS before storing at −80°C. Cells were resuspended in 500 μL lysis buffer (10 mmol/L HEPES, 0.5% NP-40, 1.5 mmol/L $MgCl_2$, 10 mmol/L KCl) with protease inhibitors and incubated on ice for 10 minutes. After centrifugation at 5,000 rpm for 5 minutes, the nuclear pellet was lysed in 500 μL nuclear lysis buffer (50 mmol/L Tris, 1% SDS, 10 mmol/L EDTA) with protease inhibitors for 15 minutes. Extracts were sonicated, cleared by centrifugation, and diluted to 1×10^6 cells per mL in dilution buffer (0.01% SDS, 1.1% Triton X-100, 1.2 mmol/L EDTA, 167 mmol/L NaCl, 16.7 mmol/L Tris). Antibody incubation (4 μg) was performed overnight. ChIP antibodies used are located in the Supplementary Material. Forty microliters of 50% Protein A/G beads (GE Healthcare) was added to lysates and rotated at 4°C for 3 hours. Protein-bound beads were sequentially washed with wash I (20 mmol/L Tris, 150 mmol/L NaCl, 2 mmol/L EDTA, 1% Triton X-100, 0.1%SDS), wash II (20 mmol/L Tris, 500 mmol/L NaCl, 2 mmol/L EDTA, 1% Triton X-100, 0.1% SDS), wash III (10 mmol/L Tris, 250 mmol/L LiCl, 1 mmol/L EDTA, 1% NP-40, 1% deoxycholate), then washed twice with TE. DNA was eluted with 1% SDS, 0.1 mol/L $NaHCO_3$ and reverse cross-linked by incubation at 65°C with RNase overnight. Eluants were then treated with proteinase K, and DNA was purified using Qiagen PCR Purification Kit. DNA amplification was performed by qPCR as described above.

Pyrosequencing

Primers for CDKN2a pyrosequencing assays were designed using PSQ assay design software version 1.0.6 (Qiagen). The primer sequences and PCR conditions are provided in the Supplementary Material. Seven microliters of PCR products were used for pyrosequencing following the protocol from the manufacturer (Qiagen).

Statistical analysis

Statistical analysis was performed using GraphPad Prism (Version 6.0). All survival curves were analyzed by log-rank (Mantel–Cox) test. IHC and immunofluorescence (IF) analyses were performed using the Mann–Whitney test. IC_{50} and growth curve determinations and significance calculations were found by nonlinear regression analysis. All other assays were performed using either paired or unpaired standard *t* test.

Results

H3.3K27M cooperates with PDGF signaling to increase tumor grade and proliferation *in vivo*

Previous studies have shown that H3.3K27M expression correlates with increased disease aggressiveness in patients and increased proliferation and stem cell characteristics *in vitro* (3, 27). In addition, some evidence suggests a nestin-positive, hedgehog-responsive progenitor within the brainstem is a candidate for the cell of origin for DIPG (28). Therefore, we utilized the RCAS/tv-a system to express the H3.3K27M mutation in nestin-expressing progenitor cells of the neonatal murine brainstem to model DIPG *in vivo* and investigate the direct protumorigenic mechanisms of H3.3K27M. We found that H3.3K27M expression alone did not induce tumors by histologic analysis of the brains (Supplementary Table S1).

PDGFB overexpression alone in our nestin tv-a murine model normally induces low-grade brainstem gliomas with the mice typically remaining asymptomatic (29). We examined the combined expression of PDGFB with H3.3K27M, H3.3WT, or empty vector to determine the impact of H3.3K27M on survival and tumor grade. All PDGFB; empty vector control mice survived to the 12-week endpoint as expected. Similarly, the majority of the PDGFB; H3.3WT control mice survived to the 12-week endpoint. Interestingly, 22% of the PDGFB; H3.3K27M–expressing mice developed tumor symptoms before the 12-week endpoint that met our criteria for sacrifice (Fig. 1A). Histologic analysis of both PDGFB; empty vector and PDGFB; H3.3WT brains showed only grade 2 tumors, while the PDGFB; H3.3K27M cohort demonstrated 47% grade 2, 47% grade 3, and 6% grade 4 tumor incidences (Fig. 1B). The grade 3–4 gliomas within the PDGFB; H3.3K27M group displayed increased microvascular proliferation, mitotic figures, and overall increased cellular density as detected by H&E staining (Fig. 1C). Consistent with these findings, PDGFB; H3.3K27M tumors harbored significantly increased EdU-positive cycling cells as compared with controls (Fig. 1C and D). Tumor volumes analyzed using MRI scans also complemented these results, revealing a trend for larger tumors with H3.3K27M expression (Supplementary Fig. S1A). Thus, H3.3K27M increases proliferation, raises tumor grade, and reduces latency of PDGFB-driven, p53 WT brainstem glioma in mice.

H3.3K27M accelerates tumorigenesis in a high-grade murine brainstem glioma model

We generated high-grade murine models of DIPG by adding RCAS-Cre–mediated p53 knockout to our PDGFB-driven tumors and expressing H3.3WT or H3.3K27M with either HA- or GFP-tags. Tumors were invasive, localized to the brainstem region, highly proliferative, and showed high expression of olig2, nestin, and the H3.3WT or H3.3K27M constructs by IHC (Fig. 2A). Power analysis for the HA-tagged model indicated that the accurate detection of a minimum 5-day survival difference would require at least 40 mice per group. With this experimental design, we found that H3.3K27M-HA mice exhibited significantly shorter tumor latency with a median survival of 36 days compared with 41 days in the H3.3WT-HA group (Fig. 2B; Supplementary Table S1). The GFP-tagged constructs showed similar results, with H3.3K27M-mutant mice succumbing to tumor an average of 8 days earlier compared with H3.3WT-GFP mice (36 and 44 days, respectively; Supplementary Fig. S1B). Analysis of H3.3WT-HA and H3.3K27M-HA tumors showed no difference in tumor cell proliferation by phosphorylated H3 (pH3) IHC or EdU immunofluorescence (Supplementary Fig. S1C and S1D).

We next derived purified primary tumor lines using FACS to isolate the GFP-tagged H3.3WT or H3.3K27M populations and cultured the cells short term in serum-free conditions for *in vitro* analysis. The GFP-purified neurospheres allow us to study the effects of H3.3K27M in isolation of the tumor bulk while better retaining *in vivo* tumor properties in an *in vitro* setting (30). We first performed Western blots to determine the level of exogenous histone overexpression and analyze H3K27me3 levels. We confirmed that H3.3K27M-expressing tumors harbored the characteristic global decrease in H3K27me3 by Western blot analysis. In addition, the exogenous GFP-tagged histones were expressed at near equal levels between H3.3K27M and H3.3WT controls and showed comparable expression with endogenous histone levels (Fig. 2C; Supplementary Fig. S1E). BrdUrd incorporation assays show that H3.3K27M cells proliferate at a significantly higher rate as compared with the H3.3WT-GFP control tumor lines (Fig. 2D). Furthermore, cell-cycle analysis comparing H3.3K27M and H3.3WT controls revealed a significant shift in the H3.3K27M lines toward the S and G_2–M phases with a corresponding reduction in the G_0–G_1 phase cells (Fig. 2E). This further indicates a higher percentage of proliferating cells in H3.3K27M-mutant lines. Taken together, these data show that expression of H3.3K27M increases tumor cell proliferation in PDGFB-driven brainstem gliomas independent of p53 status.

H3.3K27M induces localized repression of p16 expression

To elucidate potential mechanisms underlying H3.3K27M-induced increased malignancy and cell-cycle progression, we extracted tumor tissue from PDGFB; $p53^{-/-}$; empty vector control and PDGFB; $p53^{-/-}$; H3.3K27M expressing high-grade tumors and performed RNA sequencing (RNA-Seq) analysis. We found a total of 224 significantly differentially expressed genes with 182 upregulated and 42 downregulated genes in the H3.3K27M group compared with the controls (Fig. 3A; Supplementary Material). Unsupervised hierarchical clustering and principal component analysis showed H3.3K27M group tumors have a distinct gene expression profile compared with the PDGFB; $p53^{-/-}$; empty vector controls (Fig. 3A and B). Gene set enrichment analysis (GSEA) demonstrated a significant upregulation of PRC2-regulated genes from embryonic and neural progenitor (Supplementary Fig. S2A). Gene ontology (GO) using DAVID software indicated upregulated genes were enriched in neuronal function and morphogenesis as reported in DIPG patient studies (Fig. 3C; ref. 15). In addition, we used GSEA analysis to compare our mouse tumors to DIPG patient data and found varying levels of similarities (Supplementary Fig. S2B).

Intriguingly, known PRC2 target genes were also among the downregulated genes in H3.3K27M tumors, suggesting residual PRC2-induced repression despite inhibition of EZH2

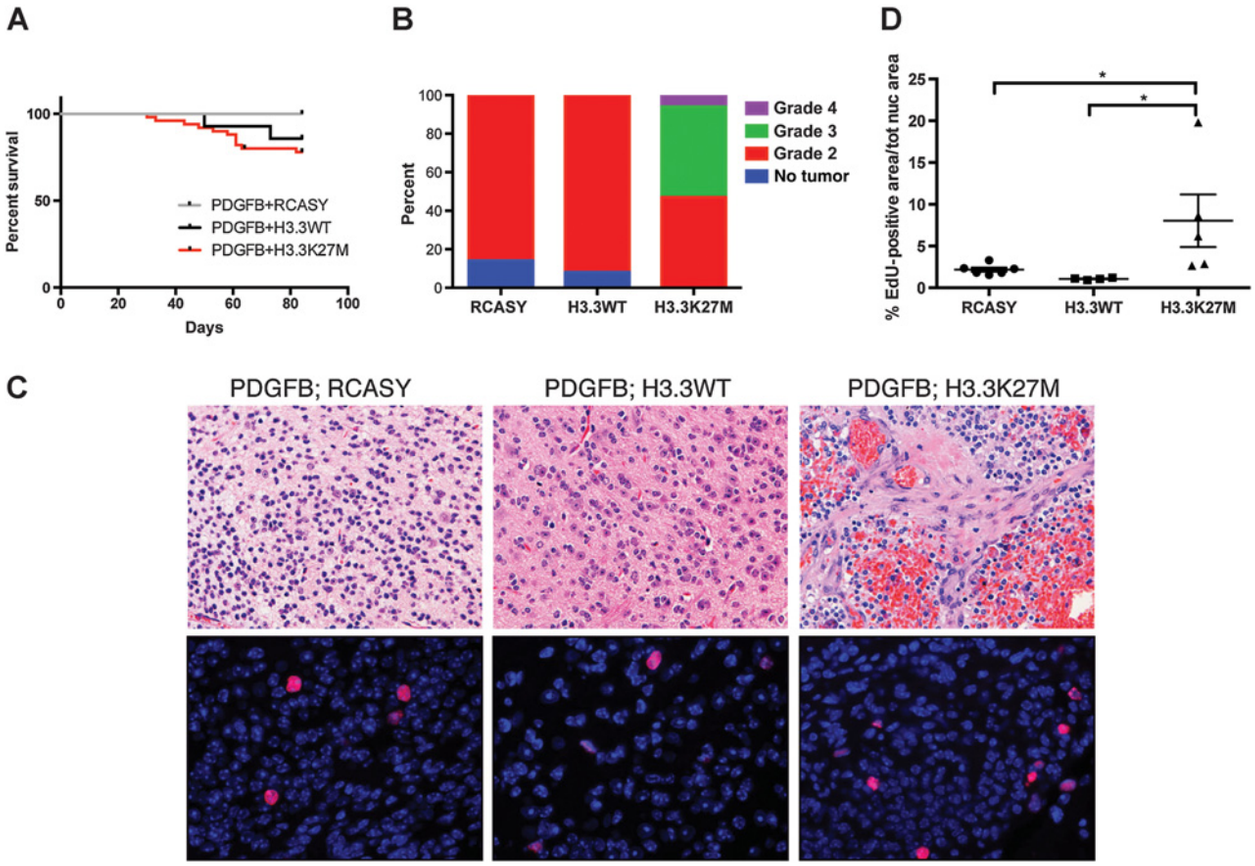

Figure 1.

H3.3K27M cooperates with PDGF signaling to increase tumor malignancy **A,** Nestin tv-a mice were injected with RCAS-PDGFB and either RCAS-Y, RCAS-H3.3WT, or RCAS-H3.3K27M. Kaplan–Meier survival curve of all three groups showing a significant difference between the PDGFB; H3.3K27M and PDGFB; RCASY groups ($N = 15$ for PDGF-B; empty vector, $N = 50$ for PDGF-B; H3.3K27M, $P = 0.048$). **B,** Graph of tumor grades for PDGFB; RCASY ($n = 7$), PDGFB; H3.3WT ($n = 13$), and PDGFB; H3.3K27M ($n = 15$). **C,** Representative H&E (40×) stained murine tumors driven by PDGFB signaling in combination with (i) RCASY empty vector, (ii) H3.3WT, or (iii) H3.3K27M (top) and IF images (40×) of these groups with EdU (red) injection 4 hours prior to sacrifice to mark proliferating cells. Total nuclei stained with DAPI (blue). **D,** IF image quantification of total EdU-positive nuclear (nuc) area over total nuclear area for PDGFB; RCASY ($n = 6$), PDGFB; H3.3WT ($n = 4$), and PDGFB; H3.3K27M ($n = 5$) groups show a significantly higher percentage of EdU-positive nuclei in PDGFB; H3.3K27M compared with both PDGFB; RCASY ($P = 0.017$) and PDGFB; H3.3WT ($P = 0.016$).

methyltransferase function by H3.3K27M. GO analysis of the downregulated genes revealed enrichment for developmental and cell-cycle–regulatory genes (Fig. 3C). The critical tumor suppressor locus *Cdkn2a* is among the H3.3K27M-repressed loci (Fig. 3C). As the *cdkn2a* locus harbors both the p16/ink4a and p19/Arf alternate transcripts, we utilized qPCR to analyze both transcripts and found specific p16 downregulation in both *in vitro*–cultured tumor cells as well as *ex vivo*–infected brainstem progenitor cells (Fig. 3D; Supplementary Fig. S2C). Thus, these results suggest the H3.3K27M mutation specifically represses p16 without altering p19 expression levels, potentially contributing to the accelerated cell-cycle progression and increased proliferation seen in our mutant tumor cells.

Aberrant increase of H3K27me3 is localized to the p16 promoter

As the *CDKN2A* locus is a known PRC2 target, we next analyzed H3K27me3 levels at the p16 promoter as a possible H3.3K27M-induced silencing mechanism (31, 32). To test this, we designed ChIP-qPCR primers for the p16 promoter, as well as the p19 promoter, p16 exon 1α, and p16 exon 2 (Fig. 4A). We then performed ChIP-qPCR for H3K27me3 on our *in vitro* GFP-purified tumor lines. We used the hoxa11, a site that is highly repressed by PRC2 in adult cells, and the β-actin promoter as positive and negative controls for our ChIP-qPCR analysis respectively and found high H3K27me3 levels in both H3.3K27M and H3.3WT cells at hoxa11, with very low levels at β-actin (Supplementary Fig. S3A). Analysis at the p16 promoter revealed that H3.3K27M significantly increased H3K27me3 levels at the p16 promoter with no significant difference at the p19 promoter (Fig. 4B). H3K27me3 analysis at p16 exon 1α and exon 2 showed trends for increased methylation (Supplementary Fig. S3B). Of note, ChIP for the GFP tag fused to H3.3WT and H3.3K27M constructs showed both exogenous histones integrated into the p16 promoter region at equal levels, and are unaffected by EZH2 inhibition, suggesting that the difference observed for H3K27me3 is not a result of reduced occupancy of the mutant oncohistone at this locus (Fig. 4C).

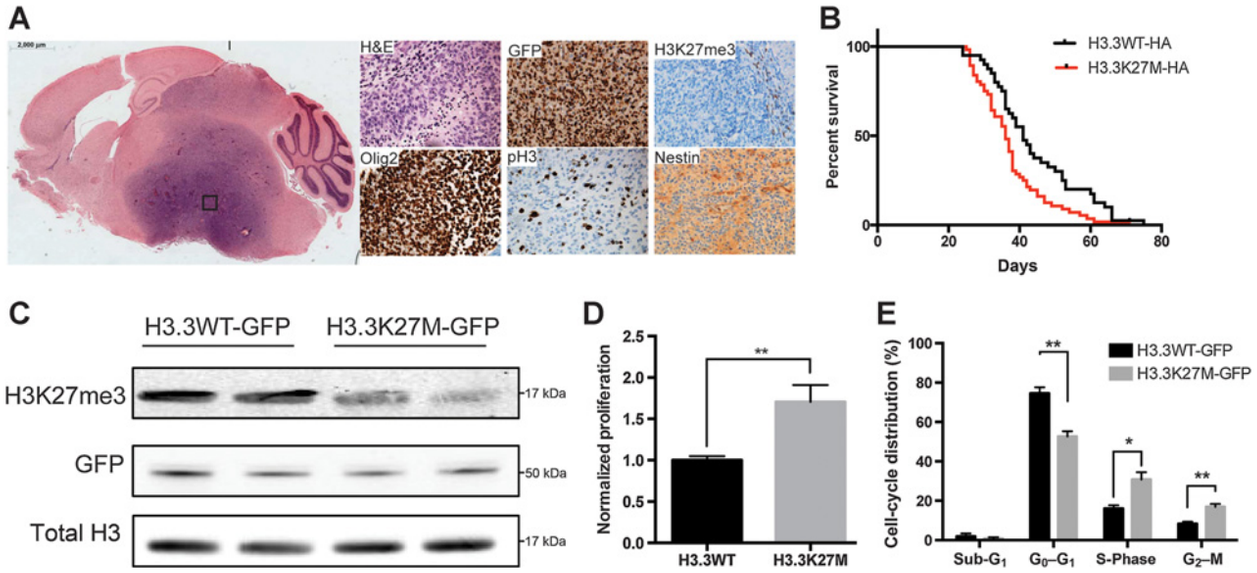

Figure 2.

H3.3K27M cooperates with PDGFB and p53 knockout to decrease survival and increase tumor cell proliferation. **A,** IHC of high-grade H3.3K27M tumor model. H&E (1×) shows lower brainstem tumor localization. Tumors show high expression of Olig2, GFP (histone tag), pH3, and nestin with low H3K27me3 at 40x. **B,** Nestin tv-a; $p53^{fl/fl}$ mice were injected with RCAS-PDGFB, RCAS-Cre, and either RCAS-H3.3WT-HA ($n = 40$) or RCAS-H3.3K27M-HA ($n = 55$). Kaplan–Meier curve of high grade PDGFB, p53 knockout tumors including either H3.3WT-HA or H3.3K27M-HA expression. K27M group shows significantly reduced survival ($P = 0.0065$). **C,** Histone extraction Western blot analysis of *in vitro*–cultured tumor-derived neurospheres for H3K27me3, GFP (fused to H3.3 RCAS constructs), and total H3 proteins. **D,** BrdUrd incorporation proliferation assay shows significantly increased proliferation in isolated H3.3K27M-GFP–expressing tumor-derived neurosphere lines ($n = 5$ each, $P = 0.003$). **E,** Cell-cycle analysis was performed on propidium iodide–stained H3.3WT or H3.3K27M-mutant murine glioma lines ($n = 3$ each). K27M-GFP–expressing lines showed a significantly reduced percentage of cells in the G_0–G_1 stage ($P = 0.006$) with corresponding increases in S- and G_2–M phases ($P = 0.02$ and $P = 0.01$, respectively).

We next treated H3.3WT or H3.3K27M murine tumor lines with two potent EZH2 inhibitors, GSK343 and EPZ6438, to test whether the increased H3K27me3 levels at the p16 promoter regulate p16 expression (33, 34). Both drugs induced global reductions in H3K27me3 levels after 7 days of 1 μmol/L treatment (Fig. 4D; Supplementary Fig. S3C). In addition, GSK343 treatment led to a specific reduction in promoter H3K27me3 at the p16 locus (Fig. 3E). Interestingly, we measured p16 promoter H3K4me3 levels with and without EZH2 inhibition by ChIP and detected the mark in both H3.3WT and H3.3K27M cells with no significant difference in the vehicles. However, there was a significant difference in the response of H3.3K27M cells to EZH2 inhibition, inducing increased H3K4me3 levels at the p16 promoter (Supplementary Fig. S4D). Surprisingly, although the EZH2 inhibitors reduced p16 H3K27me3 to near background levels and increased promoter H3K4me3, there was no corresponding rescue of p16 expression after the 7-day or with an extended 21-day treatment (Fig. 4F; Supplementary Fig. S4E). Accordingly, EZH2 inhibition with GSK343, EPZ6438, and an additional EZH2 inhibitor GSK126, did not affect proliferation of either H3.3K27M or H3.3K27M cells, with no observed IC_{50} up to 10 μmol/L (Fig. 4G; Supplementary Fig. S3F). Taken together, these data suggest that there are additional regulators involved in the H3.3K27M-induced inhibition of p16.

Inhibition of DNA methylation rescues p16 expression in H3.3K27M cells

Earlier studies provide evidence suggesting PRC2 components interact with DNA methylation machinery, recruiting them to sites of H3K27me3 silencing (35). To determine whether the increased p16 promoter H3K27me3 in H3.3K27M cells coincides with DNA methylation, we designed pyrosequencing primers for the region within the p16 promoter overlapping the ChIP-qPCR primers (Fig. 5A). Although 6 of 8 H3.3K27M and only 3 of 9 H3.3WT tumor-derived neurosphere lines exhibited higher than 20% promoter DNA methylation, there was no significant difference in the average percent methylation between the groups (Fig. 5B; Supplementary Table S2). In addition, there was no apparent increase in localization of DNMT1, which is responsible for the maintenance of DNA methylation during replication, to the p16 promoter in the H3.3K27M-expressing tumor cells (Supplementary Fig. S4A). Notably, the pharmacologic inhibition of EZH2 did not affect DNA methylation levels at the p16 promoter of both H3.3K27M and H3.3WT tumor cells (Supplementary Fig. S4B).

We next treated our *in vitro* murine tumor cells and cultured H3.3K27M-mutant DIPG patient lines with the potent DNA methyltransferase inhibitor decitabine to examine whether a reduction in promoter DNA methylation could rescue p16 expression. Treatment of tumor lines with 1 μmol/L decitabine for 72 hours significantly reduced p16 promoter DNA methylation specifically in H3.3K27M cells in both mouse and human DIPG lines (Fig. 5C; Supplementary Fig. S4C). Strikingly, this treatment significantly rescued p16 mRNA expression to near WT levels in the H3.3K27M mouse cells and resulted in increased p16 protein expression in human DIPG lines (Fig. 5D; Supplementary Fig. S4D; Supplementary Table S3). In addition, decitabine treatment exhibited a potent antiproliferative effect independent of the H3.3K27M mutation in both mouse and human lines. Treatment

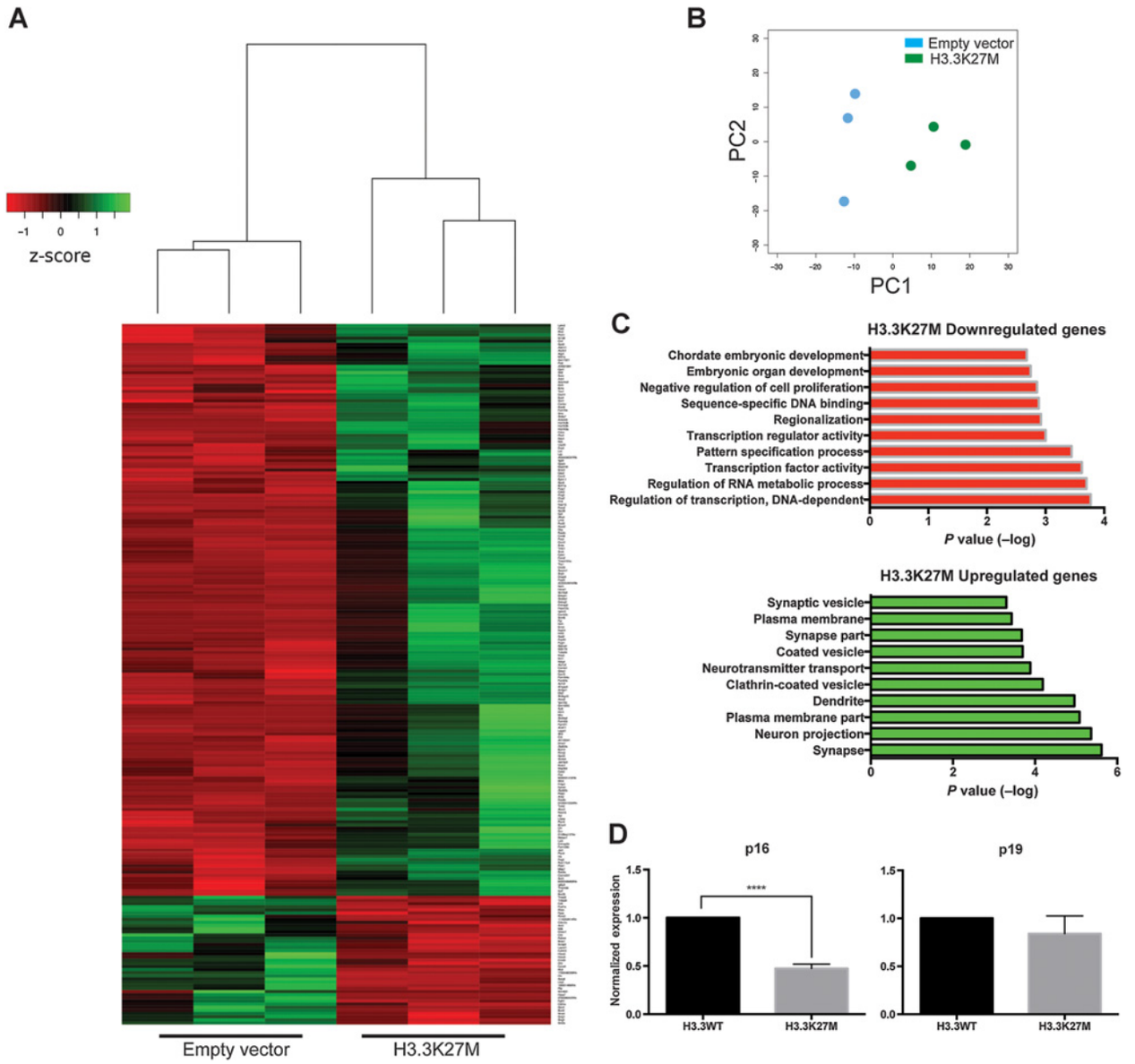

Figure 3.

H3.3K27M induces repression of p16 expression **A.** Unsupervised hierarchical clustering of differentially regulated genes ($P_{adj} < 0.05$) between H3.3K27M-overexpressing gliomas and PDGFB; p53-KO; empty vector controls ($n = 3$ each). **B,** Principal component analysis comparing PDGFB; $p53^{-/-}$; H3.3K27M and PDGFB; $p53^{-/-}$; empty vector tumors. **C,** GO pathway analysis results using DAVID software of upregulated and downregulated genes identified by RNA-Seq. **D,** qPCR validation of p16 and p19 transcript levels from murine tumor-derived *in vitro* grown neurosphere lines show H3.3K27M induces significant repression of p16 compared with H3.3WT controls ($n = 3$ each, $P < 0.0001$)

with a different DNA methyltransferase, azacitidine, showed the same effect in mouse tumor cells (Supplementary Fig. S4E). Collectively, these data suggest that DNA methylation plays a role in regulating p16 expression in H3.3K27M cells.

Loss of p16/ink4a is central to H3.3K27M-mediated increased tumor cell proliferation and malignancy

The p16 tumor suppressor is an important regulator of cell-cycle entry by inhibiting cyclin-dependent kinases 4 and 6 (CDK4/6) from phosphorylating RB protein leading to inhibition of S-phase entry (36). To determine whether the p16/RB pathway contributes to the K27M-mediated increased cell proliferation, we utilized palbociclib, a potent and specific CDK4/6 inhibitor FDA-approved for the treatment of breast cancer to specifically target the pathway (37, 38). We have previously shown that palbociclib significantly increases survival in a murine brainstem glioma model induced with PDGF-B in *cdkn2a* knockout mice (19). Therefore, tumor cells expressing the mutant histone may exhibit increased sensitivity to this drug due to the reduced p16 levels. Indeed, the IC_{50} for the H3.3K27M-expressing cells was

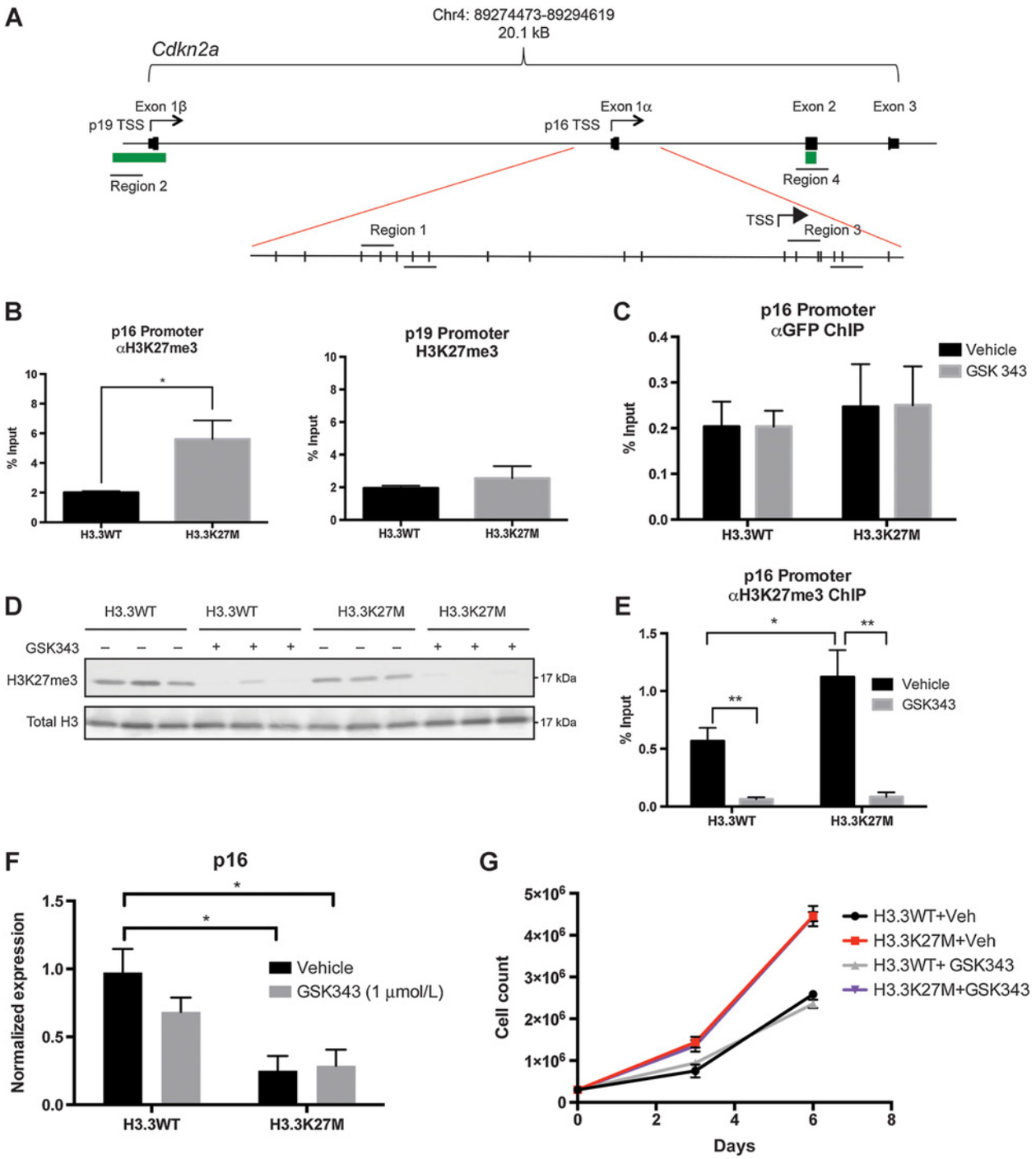

Figure 4.

H3.3K27M-induced gain of H3K27me3 at the p16 promoter. **A,** Schematic of *Cdkn2a* locus showing locations of ChIP primers for p16 and p19 promoters (region 1 and 2), as well as p16 exon 1α and exon 2 (regions 3 and 4). Green bars indicate CpG island locations B. ChIP-qPCR of H3K27me3 at the p16 and p19 promoters in cultured, high-grade murine tumor cells ($n = 3$) C. ChIP-qPCR for GFP-tagged histone constructs localized to the p16 promoter after a 7-day 1 μmol/L GSK343 or DMSO vehicle treatment ($n = 3$) **D,** Western blot analysis for H3K27me3 and total H3 of murine tumor-derived neurospheres after a 7-day treatment with either vehicle or 1 μmol/L GSK343. **E,** ChIP-qPCR of H3K27me3 at the p16 promoter of cultured tumor cells after a 7-day, 1 μmol/L GSK343 or DMSO vehicle treatment (*, $P < 0.05$; **, $P < 0.002$). **F,** qPCR for p16 expression levels in response to GSK343 or vehicle of *in vitro* murine tumor cell lines ($n = 3$/group). **G,** Cell count assay on murine tumor cell lines ($n = 3$ each) treated with 1 μmol/L GSK343 for 7 days. Growth curves were significantly different between H3.3K27M + vehicle (veh) and both H3.3WT + GSK343 and H3.3WT + vehicle ($P = 0.005$ and $P = 0.0009$, respectively). There was also a significant difference between H3.3K27M + GSK343 and both H3.3WT + GSK343 and H3.3WT + vehicle ($P = 0.006$ and $P = 0.001$, respectively).

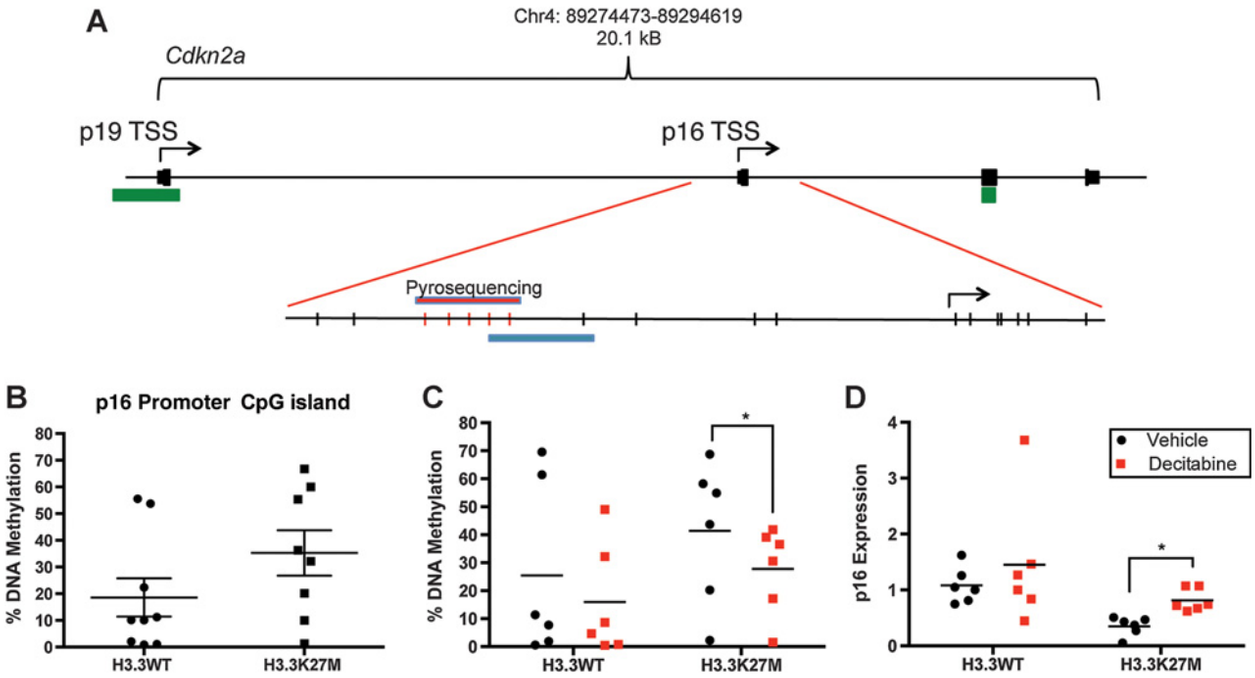

Figure 5.

The role of DNA methylation in H3.3K27M-induced p16 repression. **A,** Schematic of CpG islands (green bars) within the murine *cdkn2a* locus and pyrosequencing primer locations (blue bars). **B,** Pyrosequencing results for DNA methylation at the p16 promoter of *in vitro* H3.3WT or H3.3K27M murine tumor cells ($n = 3$, $P = 0.15$). **C,** Percent DNA methylation levels at the p16 promoter of H3.3WT and H3.3K27M murine tumor lines after 1 μmol/L decitabine treatment for 72 hours ($n = 3$, $P = 0.017$ for H3.3K27M vehicle vs. decitabine). **D,** p16 transcript expression in murine cell lines after 72-hour 1 μmol/L decitabine treatment on murine cell lines ($n = 3$, $P = 0.016$ for H3.3K27M vehicle vs. decitabine).

significantly lower as compared with the H3.3WT controls (0.18 and 1.5 μmol/L, respectively; Fig. 6A). Cell-cycle analysis of H3.3WT and H3.3K27M tumor cells treated with 2.5 μmol/L palbociclib for 48 hours showed no effect of the drug on H3.3WT cells, while the percentage of H3.3K27M cells undergoing S-phase entry was significantly reduced with the treatment (Fig. 6B).

Finally, we incorporated a *Cdkn2a* floxed allele into our RCAS murine tumor model to determine whether reduced p16 expression is a key component of H3.3K27M-mediated accelerated tumor development. We induced tumors in nestin tv-a; $cdkn2a^{fl/fl}$ mice by injection of RCAS viruses containing PDGFB, p53shRNA, and either the H3.3WT-GFP or H3.3K27M-GFP constructs along with RCAS-Cre or empty vector with the caveat that p19/Arf is also deleted in these mice. Power analysis indicated 20 mice per group were required to determine the impact of H3.3K27M in this model. We observed significantly reduced survival in the H3.3K27M-GFP group, as seen in our other H3.3K27M-expressing models, with a median survival of 37 days compared with 46 days in the H3.3WT-GFP group (Fig. 6C). Interestingly, the *cdkn2a* knockout cohorts exhibited the most aggressive tumor development with both H3.3WT- and H3.3K27M-expressing groups (median survival 30 and 32 days, respectively) displaying significantly shorter survival than the *cdkn2a* WT groups. Importantly, the H3.3K27M-induced survival difference in this DIPG model was completely abolished with knockout of *cdkn2a* (Fig. 6C). Of note, the reduced variability of the *cdkn2a* knockout models allows for sufficient power with $n = 6$ per group. Together with the increased sensitivity to CDK4/6 inhibition, this critically demonstrates that H3.3K27M-induced repression of p16 expression is a major factor in the accelerated tumor development and increased proliferating cells seen in our mutant models.

Discussion

Understanding how the hallmark H3.3K27M mutation contributes to DIPG development and progression is key in developing efficacious therapies. Our studies use genetic mouse modeling to demonstrate that H3.3K27M directly accelerates gliomagenesis by cooperating with PDGF signaling independent of p53. Furthermore, our work provides strong evidence that repression of p16 is an important component of H3.3K27M-driven gliomagenesis.

H3.3K27M cooperates with PDGF signaling and p53 loss to accelerate tumorigenesis

Previous patient studies have implicated that the presence of H3.3K27M mutation correlates with increased malignancy, decreased survival, *PDGFRA* amplifications, and *TP53* alterations (3–5). These data suggest that there is a relationship between the tumor-driving mechanisms of these alterations, and our work here along with other studies has provided evidence in favor of this (22, 27). Interestingly, our IHC analysis of the high-grade model revealed no significant difference in the percentage of proliferating cells between H3.3K27M and H3.3WT tumors. This may be a consequence of the time point in which tissue was collected, as mice were sacrificed upon reaching euthanasia criteria, at a late stage of the disease. Once cultured however, we

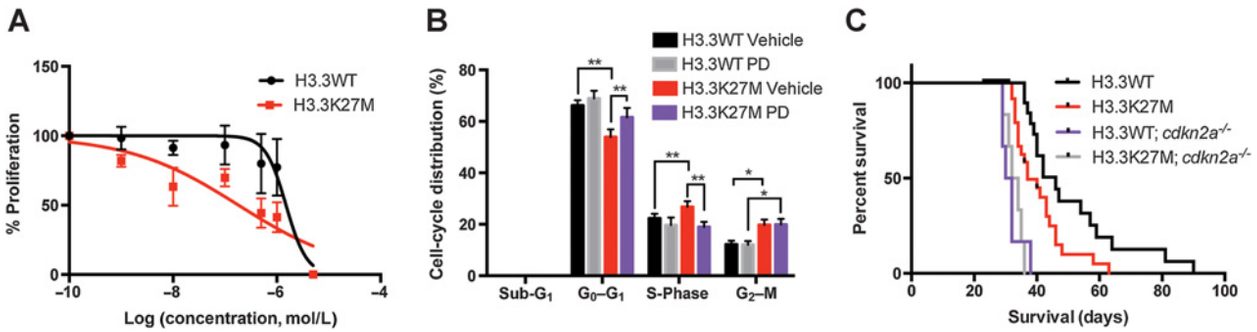

Figure 6.

Cdkn2a is central to the H3.3K27M-induced increased tumor cell proliferation and decreased tumor latency. **A,** IC_{50} determination of the CDK4/6 inhibitor palbociclib on H3.3WT-GFP or H3.3K27M-GFP murine tumor derived lines using BrdUrd incorporation. Cell lines were incubated with palbociclib for 48 hours before the assay was performed using the following concentrations: 0 nmol/L, 1 nmol/L, 10 nmol/L, 100 nmol/L, 500 nmol/L, 1 μmol/L, and 5 μmol/L. The IC_{50}s for the H3.3WT and H3.3K27M lines were calculated to be 1.5 and 0.18 μmol/L, respectively ($n = 3$ per group, $P = 0.002$). **B,** Cell-cycle analysis summary of H3.3K27M-GFP and H3.3WT-GFP FACS purified tumor-derived neurospheres treated with 2.5 μmol/L palbociclib for 48 hours (*, $P < 0.05$; **, $P < 0.009$). In addition, H3.3WT + PD versus H3.3K27M + vehicle in S- and G_2–M phases, and H3.3WT + vehicle versus H3.3K27M + PD are statistically significant ($P < 0.009$, $P < 0.05$, and $P < 0.05$, respectively). **C,** Nestin tv-a; $cdkn2a^{fl/fl}$ mice were injected with RCAS- PDGFB, RCAS- p53shRNA, and either RCAS-H3.3WT ($n = 17$) or H3.3K27M ($n = 22$), with or without RCAS-Cre ($n = 6$ for both). Kaplan–Meier survival shows significant survival differences between H3.3K27M versus H3.3WT $P = 0.016$, H3.3K27M versus H3.3K27M + $Cdkn2a^{-/-}$ $P = 0.0007$, H3.3K27M versus H3.3WT + $Cdkn2a^{-/-}$ $P = 0.0001$, H3.3WT versus H3.3K27M + $Cdkn2a^{-/-}$ $P < 0.0001$, and H3.3WT versus H3.3WT + $Cdkn2a^{-/-}$ $P < 0.0001$.

show H3.3K27M expression leads to significantly increased proliferation.

Our previous work revealed that H3.3K27M expression combined with p53 loss induced ectopic proliferating clusters, but was not sufficient to induce tumors (13). Our work here suggests the H3.3K27M mutation requires PDGF signaling as a mitogen to exert its protumorigenic effects. It remains to be seen whether the histone mutations (either H3.1 or H3.3) induce similar effects in the context of other genetic alterations, such as *PPM1D* mutations, *ACVR1* mutations, or PI3K pathway alterations, all of which are found in DIPG (39, 40).

Epigenetic mechanisms play a role in H3.3K27M-induced p16 repression

RNA-Seq analysis of our murine tumors revealed a substantial number of differentially expressed genes, including most notably a subset of repressed genes in H3.3K27M tumors. Comparing expression results from our model with human DIPG published data shows mixed results by GSEA. This could be attributed to different species, and the complex factors affecting patient samples such as treatment effects, postmortem collection, and human genetics. Nevertheless, our GO term pathways for the upregulated and downregulated genes showed enrichment in neuronal and developmental pathways, respectively, which have been reported in human studies. Importantly, the work by Chan and colleagues indirectly suggested that H3.3K27M expression induced specific p16 repression by gain of H3K27me3 using normal neural stem cells as controls. Our work adds to this by revealing that the p16 suppression is a direct result of H3.3K27M expression *in vivo*, as well as *in vitro* in both tumor-derived neurospheres and single construct expressing neuronal progenitors.

Although *CDKN2A* alteration is common to many cancers, including adult high-grade gliomas and pediatric high-grade gliomas in the cerebral cortex, it is rare in DIPG (9, 17, 41). However, our work reveals that expression of H3.3K27M may recruit epigenetic regulators to repress p16. We find that H3.3K27M induces a focal increase in p16 promoter H3K27me3, a canonically repressive epigenetic mark. A recent study has also noted the importance of H3.3K27M-induced p16 repression in DIPG using a different mouse model and human DIPG lines, but there are also notable differences (22). Mohammad and colleagues observed that inhibition of EZH2 is sufficient to restore p16 expression and inhibit cell growth. However, we show that EZH2 inhibitors do not rescue p16 expression nor inhibit proliferation at a dose that is effective at reducing the H3K27me3 gain at the p16 promoter, in our H3.3K27M murine cells. Our results are in agreement with a recent report in which EZH2 inhibitors were shown to be ineffective against human DIPG lines *in vitro*, suggesting additional repressive systems are involved (42). The discrepant observations could be due to cell-type–specific differences or could be related to p53 status of the various models as suggested by Mohammad and colleagues or other unknown factors and highlights the complexity of studying H3.3K27M mutations.

Continued p16 repression after eliminating the promoter H3K27me3 gain suggests additional regulation acting dependent or independently of the repressive histone mark. H3K27me3 is known to recruit DNA methyltransferases (DNMT) to drive *de novo* DNA methylation in certain cancers, and the *Cdkn2a* locus can be regulated by both H3K27me3 and DNA methylation of promoter CpG islands (31, 43, 44). The relationship between these epigenetic regulators is complex but interdependent (43, 45–48). This remains true in the context of H3.3K27M, as tumors from pediatric glioma patients harboring these mutations exhibit global reduction of H3K27me3 and a DNA hypomethylation profile (15). Therefore, it is possible that, in the context of H3.3K27M expression, regions of aberrant gains in H3K27me3 may also harbor increased DNA methylation providing an additional repression.

Supportive of this hypothesis here, we find that regions of DNA methylation overlap with regions of increased H3K27me3 within the p16 promoter. In addition, inhibition of DNA methylation rescued p16 expression specifically in H3.3K27M cells, although the mechanism remains unclear and warrants further study.

Regulation of DNA methylation is complex but important to tumorigenesis, as recent evidence shows that hypoxia can induce loss of TET enzyme activity, which catalyzes DNA demethylation and therefore drives DNA hypermethylation in tumors (49). However, several works have shown that PRC2 binding to H3.3K27M stalls the complex, which may increase recruitment of DNMTs to regions with H3K27M occupancy (14, 50, 51). Although we did not observe increased localization of DNMT1 to the p16 promoter, which is responsible for the maintenance of DNA methylation during replication, DNMT3A or DNMT3B, which are the only other mammalian DNMTs and perform *de novo* methylation of unmethylated, and can methylate hemi-methylated DNA, may be responsible (52). Thus, further investigation is required to determine whether the H3.3K27M-induced increase in H3K27me3 acts as a recruiting platform for DNA methylation or whether other unknown factors are involved is needed.

H3.3K27M-induced repression of p16 drives accelerated gliomagenesis

Preferential repression of p16 is known to enhance mitogenic responsiveness and promote tumor progression (44). We find the H3.3K27M-induced p16 repression imparts increased sensitivity to the CDK4/6 inhibitor palbociclib compared with H3.3WT cells. Our data indicate that palbociclib, currently in clinical trials for the 10% to 30% of patients with genetic aberrations of the RB pathway, may be effective for a much larger percentage of DIPG patients than originally presumed.

Essential to this work, genetic knockout of p16 eliminated the H3.3K27M-induced survival difference between mutant and control mice, suggesting that repression of this gene is key in H3.3K27M-enhanced gliomagenesis. Together, these findings support a mechanism whereby PDGF signaling and localized H3.3K27M-induced repression of p16 cooperate to accelerate tumor cell growth and increase malignancy in DIPG models. This work highlights rescue of p16 activity through inhibitors of DNA methylation, CDK4/6, or a combination strategy as a promising avenue for DIPG therapy that may impart additional efficacy to radiation alone.

Disclosure of Potential Conflicts of Interest

No potential conflicts of interest were disclosed.

Authors' Contributions

Conception and design: F.J. Cordero, R.E. McLendon, O.J. Becher
Development of methodology: F.J. Cordero, Z. Huang, X. He, R.E. McLendon, S.K. Murphy
Acquisition of data (provided animals, acquired and managed patients, provided facilities, etc.): F.J. Cordero, Z. Huang, C. Grenier, X. He, R.E. McLendon, S.K. Murphy, R. Hashizume
Analysis and interpretation of data (e.g., statistical analysis, biostatistics, computational analysis): F.J. Cordero, X. He, R. Hashizume
Writing, review, and/or revision of the manuscript: F.J. Cordero, Z. Huang, S.K. Murphy, O.J. Becher
Administrative, technical, or material support (i.e., reporting or organizing data, constructing databases): F.J. Cordero, C. Grenier, X. He, G. Hu, R. Hashizume
Study supervision: R. Hashizume, O.J. Becher
Other (pyrosequencing assay design and data interpretation): Z. Huang

Acknowledgments

The authors thank Drs. Michelle Monje and Angel Montero Carcaboso for sharing their DIPG human cell lines, David Corcoran and the Duke Genomic Analysis and Bioinformatics Core for their help with RNA-Seq analysis, Yasheng Gao for microscopy support, the Duke Cancer Center Flow Cytometry Core for their aid with FACS and cell-cycle analysis, and the Armstrong, Linardic, and Wechsler laboratories for discussions. They also thank Katherine Misuraca and Emily Miller for their help with editing and discussions. The RCAS-p53shRNA was generously provided by the Holland laboratory. MRI was performed at the Duke Center for In Vivo Microscopy, an NIBIB National Biomedical Technology Resource Center (4 P41 EB015897).

Grant Support

This work was supported by NIH grant NS093986-01 (to F.J. Cordero), K02 award NS086917 (to O.J. Becher), the Damon Runyon Cancer Research Foundation (to O.J. Becher), and the Rory David Deutsch Foundation (to O.J. Becher).

The costs of publication of this article were defrayed in part by the payment of page charges. This article must therefore be hereby marked *advertisement* in accordance with 18 U.S.C. Section 1734 solely to indicate this fact.

Received November 3, 2016; revised April 7, 2017; accepted May 15, 2017; published OnlineFirst May 18, 2017.

References

1. Donaldson SS, Laningham F, Fisher PG. Advances toward an understanding of brainstem gliomas. J Clin Oncol 2006;24:1266–72.
2. Hargrave D, Bartels U, Bouffet E. Diffuse brainstem glioma in children: critical review of clinical trials. Lancet Oncol 2006;7:241–8.
3. Khuong-Quang DA, Buczkowicz P, Rakopoulos P, Liu XY, Fontebasso AM, Bouffet E, et al. K27M mutation in histone H3.3 defines clinically and biologically distinct subgroups of pediatric diffuse intrinsic pontine gliomas. Acta Neuropathol 2012;124:439–47.
4. Schwartzentruber J, Korshunov A, Liu XY, Jones DT, Pfaff E, Jacob K, et al. Driver mutations in histone H3.3 and chromatin remodelling genes in paediatric glioblastoma. Nature 2012;482:226–31.
5. Sturm D, Witt H, Hovestadt V, Khuong-Quang DA, Jones DT, Konermann C, et al. Hotspot mutations in H3F3A and IDH1 define distinct epigenetic and biological subgroups of glioblastoma. Cancer Cell 2012;22:425–37.
6. Wu G, Broniscer A, McEachron TA, Lu C, Paugh BS, Becksfort J, et al. Somatic histone H3 alterations in pediatric diffuse intrinsic pontine gliomas and non-brainstem glioblastomas. Nat Genet 2012;44:251–3.
7. Castel D, Philippe C, Calmon R, Le Dret L, Truffaux N, Boddaert N, et al. Histone H3F3A and HIST1H3B K27M mutations define two subgroups of diffuse intrinsic pontine gliomas with different prognosis and phenotypes. Acta Neuropathol 2015;130:815–27.
8. Wu G, Diaz AK, Paugh BS, Rankin SL, Ju B, Li Y, et al. The genomic landscape of diffuse intrinsic pontine glioma and pediatric non-brainstem high-grade glioma. Nat Genet 2014;46:444–50.
9. Paugh BS, Qu C, Jones C, Liu Z, Adamowicz-Brice M, Zhang J, et al. Integrated molecular genetic profiling of pediatric high-grade gliomas reveals key differences with the adult disease. J Clin Oncol 2010;28:3061–8.
10. Puget S, Philippe C, Bax DA, Job B, Varlet P, Junier MP, et al. Mesenchymal transition and PDGFRA amplification/mutation are key distinct oncogenic events in pediatric diffuse intrinsic pontine gliomas. PLoS One 2012;7:e30313.
11. Paugh BS, Zhu X, Qu C, Endersby R, Diaz AK, Zhang J, et al. Novel oncogenic PDGFRA mutations in pediatric high-grade gliomas. Cancer Res 2013;73:6219–29.
12. Bjerke L, Mackay A, Nandhabalan M, Burford A, Jury A, Popov S, et al. Histone H3.3. mutations drive pediatric glioblastoma through upregulation of MYCN. Cancer Discov 2013;3:512–9.
13. Lewis PW, Muller MM, Koletsky MS, Cordero F, Lin S, Banaszynski LA, et al. Inhibition of PRC2 activity by a gain-of-function H3 mutation found in pediatric glioblastoma. Science 2013;340:857–61.

14. Chan KM, Fang D, Gan H, Hashizume R, Yu C, Schroeder M, et al. The histone H3.3K27M mutation in pediatric glioma reprograms H3K27 methylation and gene expression. Genes Dev 2013;27:985–90.
15. Bender S, Tang Y, Lindroth AM, Hovestadt V, Jones DT, Kool M, et al. Reduced H3K27me3 and DNA hypomethylation are major drivers of gene expression in K27M mutant pediatric high-grade gliomas. Cancer Cell 2013;24:660–72.
16. Sturm D, Bender S, Jones DT, Lichter P, Grill J, Becher O, et al. Paediatric and adult glioblastoma: multiform (epi)genomic culprits emerge. Nat Rev Cancer 2014;14:92–107.
17. Paugh BS, Broniscer A, Qu C, Miller CP, Zhang J, Tatevossian RG, et al. Genome-wide analyses identify recurrent amplifications of receptor tyrosine kinases and cell-cycle regulatory genes in diffuse intrinsic pontine glioma. J Clin Oncol 2011;29:3999–4006.
18. von Werder A, Seidler B, Schmid RM, Schneider G, Saur D. Production of avian retroviruses and tissue-specific somatic retroviral gene transfer in vivo using the RCAS/TVA system. Nat Protoc 2012;7:1167–83.
19. Barton KL, Misuraca K, Cordero F, Dobrikova E, Min HD, Gromeier M, et al. PD-0332991, a CDK4/6 inhibitor, significantly prolongs survival in a genetically engineered mouse model of brainstem glioma. PLoS One 2013;8:e77639.
20. Grasso CS, Tang Y, Truffaux N, Berlow NE, Liu L, Debily MA, et al. Functionally defined therapeutic targets in diffuse intrinsic pontine glioma. Nat Med 2015;21:827.
21. Hashizume R, Smirnov I, Liu S, Phillips JJ, Hyer J, McKnight TR, et al. Characterization of a diffuse intrinsic pontine glioma cell line: implications for future investigations and treatment. J Neurooncol 2012;110:305–13.
22. Mohammad F, Weissmann S, Leblanc B, Pandey DP, Hojfeldt JW, Comet I, et al. EZH2 is a potential therapeutic target for H3K27M-mutant pediatric gliomas. Nat Med 2017;23:483–92.
23. Misuraca KL, Barton KL, Chung A, Diaz AK, Conway SJ, Corcoran DL, et al. Pax3 expression enhances PDGF-B-induced brainstem gliomagenesis and characterizes a subset of brainstem glioma. Acta Neuropathol Commun 2014;2:134.
24. Flicek P, Amode MR, Barrell D, Beal K, Brent S, Carvalho-Silva D, et al. Ensembl 2012. Nucleic Acids Res 2012;40:D84–90.
25. Anders S, Huber W. Differential expression analysis for sequence count data. Genome Biol 2010;11:R106.
26. Livak KJ, Schmittgen TD. Analysis of relative gene expression data using real-time quantitative PCR and the 2(-Delta Delta C(T)) Method. Methods 2001;25:402–8.
27. Funato K, Major T, Lewis PW, Allis CD, Tabar V. Use of human embryonic stem cells to model pediatric gliomas with H3.3K27M histone mutation. Science 2014;346:1529–33.
28. Monje M, Mitra SS, Freret ME, Raveh TB, Kim J, Masek M, et al. Hedgehog-responsive candidate cell of origin for diffuse intrinsic pontine glioma. Proc Natl Acad Sci U S A 2011;108:4453–8.
29. Becher OJ, Hambardzumyan D, Walker TR, Helmy K, Nazarian J, Albrecht S, et al. Preclinical evaluation of radiation and perifosine in a genetically and histologically accurate model of brainstem glioma. Cancer Res 2010;70:2548–57.
30. Lee J, Kotliarova S, Kotliarov Y, Li A, Su Q, Donin NM, et al. Tumor stem cells derived from glioblastomas cultured in bFGF and EGF more closely mirror the phenotype and genotype of primary tumors than do serum-cultured cell lines. Cancer Cell 2006;9:391–403.
31. Kotake Y, Cao R, Viatour P, Sage J, Zhang Y, Xiong Y. pRB family proteins are required for H3K27 trimethylation and Polycomb repression complexes binding to and silencing p16INK4alpha tumor suppressor gene. Genes Dev 2007;21:49–54.
32. Jacobs JJ, Kieboom K, Marino S, DePinho RA, van Lohuizen M. The oncogene and Polycomb-group gene bmi-1 regulates cell proliferation and senescence through the ink4a locus. Nature 1999;397:164–8.
33. Knutson SK, Kawano S, Minoshima Y, Warholic NM, Huang KC, Xiao Y, et al. Selective inhibition of EZH2 by EPZ-6438 leads to potent antitumor activity in EZH2-mutant non-Hodgkin lymphoma. Mol Cancer Ther 2014;13:842–54.
34. Poirier JT, Gardner EE, Connis N, Moreira AL, de Stanchina E, Hann CL, et al. DNA methylation in small cell lung cancer defines distinct disease subtypes and correlates with high expression of EZH2. Oncogene 2015;34:5869–78.
35. Vire E, Brenner C, Deplus R, Blanchon L, Fraga M, Didelot C, et al. The Polycomb group protein EZH2 directly controls DNA methylation. Nature 2006;439:871–4.
36. Harbour JW, Luo RX, Dei Santi A, Postigo AA, Dean DC. Cdk phosphorylation triggers sequential intramolecular interactions that progressively block Rb functions as cells move through G1. Cell 1999;98:859–69.
37. Flaherty KT, Lorusso PM, Demichele A, Abramson VG, Courtney R, Randolph SS, et al. Phase I, dose-escalation trial of the oral cyclin-dependent kinase 4/6 inhibitor PD 0332991, administered using a 21-day schedule in patients with advanced cancer. Clin Cancer Res 2012;18:568–76.
38. Turner NC, Huang Bartlett C, Cristofanilli M. Palbociclib in hormone-receptor-positive advanced breast cancer. N Engl J Med 2015;373:1672–3.
39. Buczkowicz P, Hoeman C, Rakopoulos P, Pajovic S, Letourneau L, Dzamba M, et al. Genomic analysis of diffuse intrinsic pontine gliomas identifies three molecular subgroups and recurrent activating ACVR1 mutations. Nat Genet 2014;46:451–6.
40. Taylor KR, Mackay A, Truffaux N, Butterfield YS, Morozova O, Philippe C, et al. Recurrent activating ACVR1 mutations in diffuse intrinsic pontine glioma. Nat Genet 2014;46:457–61.
41. Brennan CW, Verhaak RG, McKenna A, Campos B, Noushmehr H, Salama SR, et al. The somatic genomic landscape of glioblastoma. Cell 2013;155:462–77.
42. Wiese M, Schill F, Sturm D, Pfister S, Hulleman E, Johnsen SA, et al. No significant cytotoxic effect of the EZH2 inhibitor tazemetostat (EPZ-6438) on pediatric glioma cells with wildtype histone 3 or mutated histone 3.3. Klin Padiatr 2016;228:113–7.
43. Schlesinger Y, Straussman R, Keshet I, Farkash S, Hecht M, Zimmerman J, et al. Polycomb-mediated methylation on Lys27 of histone H3 pre-marks genes for de novo methylation in cancer. Nat Genet 2007;39:232–6.
44. Sharpless NE, Bardeesy N, Lee KH, Carrasco D, Castrillon DH, Aguirre AJ, et al. Loss of p16Ink4a with retention of p19Arf predisposes mice to tumorigenesis. Nature 2001;413:86–91.
45. Gal-Yam EN, Egger G, Iniguez L, Holster H, Einarsson S, Zhang X, et al. Frequent switching of Polycomb repressive marks and DNA hypermethylation in the PC3 prostate cancer cell line. Proc Natl Acad Sci U S A 2008;105:12979–84.
46. Keshet I, Schlesinger Y, Farkash S, Rand E, Hecht M, Segal E, et al. Evidence for an instructive mechanism of *de novo* methylation in cancer cells. Nat Genet 2006;38:149–53.
47. Ohm JE, McGarvey KM, Yu X, Cheng L, Schuebel KE, Cope L, et al. A stem cell-like chromatin pattern may predispose tumor suppressor genes to DNA hypermethylation and heritable silencing. Nat Genet 2007;39:237–42.
48. Widschwendter M, Fiegl H, Egle D, Mueller-Holzner E, Spizzo G, Marth C, et al. Epigenetic stem cell signature in cancer. Nat Genet 2007;39:157–8.
49. Thienpont B, Steinbacher J, Zhao H, D'Anna F, Kuchnio A, Ploumakis A, et al. Tumour hypoxia causes DNA hypermethylation by reducing TET activity. Nature 2016;537:63–8.
50. Justin N, Zhang Y, Tarricone C, Martin SR, Chen S, Underwood E, et al. Structural basis of oncogenic histone H3K27M inhibition of human polycomb repressive complex 2. Nat Commun 2016;7:11316.
51. Jiao L, Liu X. Structural basis of histone H3K27 trimethylation by an active polycomb repressive complex 2. Science 2015;350:aac4383.
52. Jackson M, Krassowska A, Gilbert N, Chevassut T, Forrester L, Ansell J, et al. Severe global DNA hypomethylation blocks differentiation and induces histone hyperacetylation in embryonic stem cells. Mol Cell Biol 2004;24:8862–71.

Neuro-Oncology

22(9), 1302–1314, 2020 | doi:10.1093/neuonc/noaa058 | Advance Access date 13 March 2020

Pharmacologic inhibition of lysine-specific demethylase 1 as a therapeutic and immune-sensitization strategy in pediatric high-grade glioma

Cavan P. Bailey, Mary Figueroa, Achintyan Gangadharan, Yanwen Yang, Megan M. Romero, Bridget A. Kennis, Sridevi Yadavilli, Verlene Henry, Tiara Collier, Michelle Monje, Dean A. Lee, Linghua Wang, Javad Nazarian, Vidya Gopalakrishnan, Wafik Zaky, Oren J. Becher, and Joya Chandra

Department of Pediatrics, Research (C.P.B., M.F., A.G., Y.Y., B.A.K., V.G., W.Z., J.C.) and Department of Epigenetics and Molecular Carcinogenesis, The MD Anderson Cancer Center, Houston, Texas (C.P.B., M.F., A.G., J.C.); Department of Pediatrics, Northwestern Feinberg School of Medicine, Chicago, Illinois (M.M.R., O.J.B.); Brain Tumor Center, The MD Anderson Cancer Center, Houston, Texas (V.H., T.C.); Department of Neurology and Neurological Sciences, Stanford University, Palo Alto, California (M.M.); Department of Pediatrics, Nationwide Children's and the Ohio State Comprehensive Cancer Center, Columbus, Ohio (D.A.L.); Department of Genomic Medicine, The MD Anderson Cancer Center, Houston, Texas (L.W.); Center for Genetic Medicine Research, Children's National Hospital, Washington, DC (S.Y., J.N.); The University of Texas MD Anderson Cancer Center UTHealth Graduate School of Biomedical Sciences, Houston, Texas (C.P.B., M.F., L.W., V.G., J.C.); Center for Cancer Epigenetics, The MD Anderson Cancer Center, Houston, Texas (C.P.B., M.F, V.G., J.C.)

Corresponding Author: Joya Chandra, PhD, Box 853 – Department of Pediatrics Research, 1515 Holcombe Blvd, Houston, TX 77030 (jchandra@mdanderson.org)

Abstract

Background. Diffuse midline gliomas (DMG), including brainstem diffuse intrinsic pontine glioma (DIPG), are incurable pediatric high-grade gliomas (pHGG). Mutations in the H3 histone tail (H3.1/3.3-K27M) are a feature of DIPG, rendering them therapeutically sensitive to small-molecule inhibition of chromatin modifiers. Pharmacological inhibition of lysine-specific demethylase 1 (LSD1) is clinically relevant but has not been carefully investigated in pHGG or DIPG.

Methods. Patient-derived DIPG cell lines, orthotopic mouse models, and pHGG datasets were used to evaluate effects of LSD1 inhibitors on cytotoxicity and immune gene expression. Immune cell cytotoxicity was assessed in DIPG cells pretreated with LSD1 inhibitors, and informatics platforms were used to determine immune infiltration of pHGG.

Results. Selective cytotoxicity and an immunogenic gene signature were established in DIPG cell lines using clinically relevant LSD1 inhibitors. Pediatric HGG patient sequencing data demonstrated survival benefit of this LSD1-dependent gene signature. Pretreatment of DIPG with these inhibitors increased lysis by natural killer (NK) cells. Catalytic LSD1 inhibitors induced tumor regression and augmented NK cell infusion in vivo to reduce tumor burden. CIBERSORT analysis of patient data confirmed NK infiltration is beneficial to patient survival, while CD8 T cells are negatively prognostic. Catalytic LSD1 inhibitors are nonperturbing to NK cells, while scaffolding LSD1 inhibitors are toxic to NK cells and do not induce the gene signature in DIPG cells.

Conclusions. LSD1 inhibition using catalytic inhibitors is selectively cytotoxic and promotes an immune gene signature that increases NK cell killing in vitro and in vivo, representing a therapeutic opportunity for pHGG.

Key Points

1. LSD1 inhibition using several clinically relevant compounds is selectively cytotoxic in DIPG and shows in vivo efficacy as a single agent.
2. An LSD1-controlled gene signature predicts survival in pHGG patients and is seen in neural tissue from LSD1 inhibitor–treated mice.
3. LSD1 inhibition enhances NK cell cytotoxicity against DIPG in vivo and in vitro with correlative genetic biomarkers.

Importance of the Study

Herein we demonstrate selective cytotoxicity of several clinically relevant LSD1 inhibitors against patient-derived DIPG cells and efficacy in 3 separate orthotopic mouse models. We define an immune gene signature that is upregulated in DIPG cells by catalytic inhibitors of LSD1. This immune gene signature is predictive of prognosis in pHGG patient datasets, consistent with the concept of LSD1 inhibition potentially improving outcomes. NK cell killing of DIPG is enhanced by LSD1 inhibition in vitro and in vivo, providing functional confirmation of this gene signature, and represents the first report of LSD1 inhibition promoting NK cell cytotoxicity of cancer cells. Given the poor prognosis of pHGGs and lack of effective treatments, our results suggest that use of LSD1 inhibition as a single agent or in combination with NK cell therapy may be a safe and efficacious strategy.

Pediatric high-grade gliomas (pHGGs) are pathologically diverse yet uniformly highly malignant central nervous system (CNS) cancers, with 5-year survival rates of <10% postdiagnosis. Surgery is often not possible due to tumor diffusion and the sensitive midline brain structure, which control crucial motor functions such as breathing and heartbeat. Radiotherapy is the standard of care, but survival benefits are slim, with high risks of side effects and decreased quality of life during and after treatment.[1] Immunotherapeutic approaches have had limited success due to the low mutational burden and immunosuppressive microenvironment of pediatric brain tumors, such that adaptive immune interventions including checkpoint blockade are ineffective.[2] Recent efforts to molecularly profile pHGGs have discovered conserved genomic mutations unique to the pediatric age range and anatomic locations.[3] In particular, mutations in histone encoding genes (*H3F3A, HIST1H3B*) resulting in amino acid substitution of the epigenetically critical lysine residue (H3-K27M) are thought to drive early development of these tumors in multipotent CNS cells.[4] As such, the World Health Organization now recognizes these K27M tumors as separate entities in the glioma classification.[5]

The K27M histone mutations present a therapeutic opportunity for the use of epigenetic regulating drugs, in particular those that target chromatin-modifying proteins. Multiple publications have explored this idea, using inhibitors of histone deacetylases (HDACs),[6] demethylases (JMJD3 [Jumonji domain]/UTX [ubiquitously transcribed tetratricopeptide repeat, X chromosome]),[7] methyltransferases (enhancer of zeste homolog 2),[8] and chromatin readers (bromodomain and extra terminal)[9] to demonstrate tumor regression in preclinical models. Clinically translatable compounds exist to target all of these and indeed an ongoing clinical trial is testing the HDAC inhibitor panobinostat as a monotherapy (NCT02717455).[10] However, other chromatin modifiers have yet to be explored as therapeutic targets, and there is limited investigation into how the gene expression changes generated by these drugs can be used to augment preexisting therapies.

The histone demethylase LSD1 removes mono- and dimethyl marks from H3K4 and H3K9 and shares structural homology with monoamine oxidases (MAOs). LSD1 is targeted by several drugs[11] and has thus far been therapeutically investigated in cancers, including acute myeloid leukemia,[12] sarcoma,[13] and neuroblastoma.[14] LSD1 inhibition has been shown to have an enticing therapeutic window that is selective for cancer cells, in part through its disruption of oncogenic and onco-maintenance transcriptional programs.[15,16] Furthermore, the H3K4me1 histone mark regulated by LSD1 was seen to be enriched in intergenic regions of pHGG cells,[9] suggesting that LSD1 may control access to enhancers of genes important in pHGG pathology. LSD1 inhibitors can functionally target either the catalytic domain that mediates demethylation[17] or the scaffolding tower domain that interfaces with other proteins in epigenetic complexes,[18] and it is currently unknown what phenotype these disparate inhibitors would produce in pHGG. Given the highly disrupted yet therapeutically sensitive epigenome of pHGGs, we sought to explore in this study whether LSD1 inhibition could both be cytotoxic to pHGG and generate transcriptional changes that would inform combination therapies.

Our group previously published a report on use of a combination therapy of LSD1 and HDAC inhibition to synergistically induce cell death in adult glioblastoma cell lines and patient-derived glial stem cells.[19] In a follow-up study, we used RNA sequencing (RNA-Seq) to explore how the HDAC/LSD1 inhibitor combination therapy produced gene changes in the p53 family members p63 and p73.[20] In our

current study, we identify an LSD1-induced immunogenic gene signature conserved in pHGG patients[21] that predicts longer survival. We further show that LSD1 inhibition is selectively cytotoxic to DIPG cells, and inhibitor-based induction of this gene signature augments innate immune reactivity against DIPG by boosting natural killer (NK) cell immunotherapy response in vitro and in vivo.

Materials and Methods

Detailed experimental procedures are provided in the Supplementary Material.

Cells and Human Samples

Human pHGG cells (DIPG IV, IV-luc, VI, and XIII) were cultured in TSM Base medium. DIPG IV and IV-luc possess a H3.1-K27M mutation, DIPG VI and DIPG XIII are H3.3-K27M mutated. LN18, U87, and immortalized normal human astrocyte (NHA) cells were cultured in fetal bovine serum–supplemented DMEM/F12 medium. Pediatric K27M cells–hemagglutinin (PKC-HA) and PKC-luciferase (luc) cells were cultured in NeuroCult medium. Human T cells were cultured in ImmunoCult-XF T-cell Expansion Medium. Human NK cells were cultured as previously described.[22]

Clinical Datasets and Bioinformatics

Gene expression in pHGGs was analyzed from the dataset published by Mackay et al[21] using the cBioPortal interface. CIBERSORT analysis, an in silico method to determine immune cell infiltrate in bulk sequenced tissue, was performed as previously described[23] using the standard LM22 leukocyte signature matrix in the same patient dataset.[21]

Mouse Models of Hemispheric pHGG and Brainstem DIPG

Nonobese diabetic severe combined immunodeficient gamma (NSG) mice were orthotopically implanted with either 500 000 DIPG IV-luc or 300 000 PKC-luc cells as a model of hemispheric pHGG. C57BL/6 mice were injected in the brainstem with 500 000 PKC-HA cells as a model of brainstem DIPG.

Cellular Thermal Shift Assay

Cells were treated for 1 h with LSD1 inhibitors, harvested and subjected to a 3 min melt curve in a thermocycler, then lysed for analysis via western blot.

NK and T-Cell Cytotoxicity Co-Culture

Target cells were labeled with calcein acetoxymethyl (AM), incubated at effector-to-target ratios of 10:1 and below, then co-incubated with effector cells (NK or T cells) for 4 h. Lysed cells release calcein AM into the supernatant, which was read on a plate reader.

Seahorse Metabolic Assays

NK and T cells were subjected to the XF Mito Stress Test on a Seahorse XFe96 using the default protocol, and 300 000 live cells per well adhered with CellTak.

Chemicals and Antibodies

Small-molecule LSD1 inhibitors were suspended and stored at –20°C in dimethyl sulfoxide (DMSO) or phosphate buffered saline (PBS) as appropriate. Antibodies were stored at 4°C or –20°C as appropriate.

Drug Screening

DIPG and NHA cells were plated in 96-well plates and dosed at indicated amounts with LSD1 inhibitors. Plates were incubated for 5 days and alamarBlue readout was measured fluorometrically on a plate reader.

Cell Viability and Apoptosis Assays

Cells were treated with LSD1 inhibitors for 72 or 96 h and harvested for analysis via trypan blue exclusion assay. Cells were also fixed with ice-cold 100% ethanol for later analysis with propidium iodide via flow cytometry.

RNA Isolation and Real-Time Quantitative PCR

RNA was extracted from cells after 24 h LSD1 inhibitor treatment and converted to cDNA, which was used directly in quantitative (q)PCR experiments to measure gene expression relative to DMSO control. Primer sequences are provided in the Supplementary Material.

Flow Cytometry

After LSD1 inhibitor treatment, cells were harvested and stained with a viability dye and antibodies for analysis via flow cytometry.

Cell Transfections

NHA and DIPG IV cells were transfected with LSD1 small interfering (si)RNA using Lipofectamine and harvested after 48 h for analysis via western blot and qPCR.

Western Blotting

Cells were lysed in radioimmunoprecipitation assay buffer and loaded onto polyacrylamide gels and subjected to electrophoresis. Proteins were transferred to polyvinylidene difluoride membranes for detection via horseradish

peroxidase–conjugated antibodies which were detected with a ChemiDocTouch.

Statistical Analysis

All statistical analysis was performed in GraphPad Prism 8.

Results

We previously performed RNA-Seq[20] on LN18 adult glioblastoma cells when LSD1 was knocked down with short hairpin (sh)RNA in order to explore the mechanism of their sensitivity to dual LSD1 and HDAC inhibition. In the LSD1 shRNA group alone, we applied a 1.5-fold change filter and analyzed the remaining genes with pathway analysis by DAVID (Database for Annotation, Visualization and Integrated Discovery) (Figure 1A). The third most significantly changed pathway was "immune response," with 24 genes upregulated and downregulated by LSD1 knockdown compared with a scramble control. We sought to validate these gene changes in LN18 cells, and replicated LSD1 knockdown in the cells and confirmed knockdown with western blot. Expression of the 13 most upregulated genes was measured with real time (RT)-qPCR and we observed a significant increase (ANOVA, $P < 0.0001$) in the gene expression signature with LSD1 knockdown (Figure 1B). This confirmed our RNA-Seq data that LSD1 controls expression of these genes in a glioblastoma cell line. Furthermore, this gene signature matches treatment of LN18 with the established LSD1 inhibitor tranylcypromine (TCP) (Figure 1B), and TCP treatment of LN18 compared with DIPG cells was nonsignificant (Figure 1C), indicating concordance of these upregulated immune genes between pediatric and adult glioma in vitro models. To determine the significance of this signature to patient treatment, we next proceeded to probe a dataset of 247 pHGG patients (Figure 1D). Expression of LSD1 was significantly lower in patients with high expression of our identified gene signature panel, suggesting that LSD1 may influence expression of these genes in pHGG patients (Figure 1E). We found our gene signature of immune response genes could predict significantly improved 5-year survival in all tumors (Figure 1F). The overall benefit was driven by K27M midline (thalamus, cerebellum, spinal cord, ventricles; $n = 23$) and wild-type (WT) hemispheric (cerebral hemispheres; $n = 57$) tumors; notably, this survival benefit did not extend to K27M brainstem (pons, midbrain, medulla; $n = 49$) tumors, and we lacked statistical power in WT brainstem ($n = 9$) and WT midline ($n = 14$) tumor samples to make strong conclusions (Figure 1F).

In order to explore the potential of therapeutically triggering this gene signature, we profiled the potency of 3 irreversible catalytic LSD1 inhibitors (tranylcypromine [TCP], GSK LSD1, and RN-1) and 2 reversible scaffolding LSD1 inhibitors (SP-2509 and SP-2577). As we have previously published, LSD1 inhibition alone in adult glioblastoma cells does not potently reduce viability.[19,20] In pHGG cells, the same inhibitors display much greater potency that correlates with their specificity and sensitivity for inhibition of LSD1 over the related proteins LSD2, MAO-A, and MAO-B. We observed highly similar half-maximal inhibitory concentration (IC_{50}) values between the unique DIPG cell types for each LSD1 inhibitor tested (Figure 2A–C). While alamarBlue screening is a sensitive assay for cell proliferation, it cannot determine if drugs are cytostatic or cytotoxic due to its reliance on metabolic activity. Therefore, we used trypan blue (membrane integrity) and propidium iodide stain (DNA fragmentation) assays to quantify cell death at the IC_{50} observed with alamarBlue (TCP: ~1.5 mM, GSK LSD1: ~400 μM, RN-1: ~60 μM, SP-2509/2577: ~13 μM). Cell death was selectively induced in DIPG cells over NHA beginning at 3 days posttreatment (Figure 2D). For neurosphere-forming DIPG XIII cells, we adapted another high-throughput technique to quantify cell death by use of the DNA-binding dye GelGreen and observed the same effects. In order to ascertain in vivo efficacy, luciferase labeled murine pHGG PKC-luc cells were implanted intracranially into NSG mice which were treated intraperitoneally 4 times weekly with vehicle, LSD1 catalytic (TCP and GSK LSD1), or LSD1 scaffolding (SP-2577) inhibitors. Noninvasive imaging showed reduction of tumor burden in mice treated with GSK LSD1 (Figure 2E, F) but not TCP or SP-2577. GSK LSD1 provides an initial survival benefit over vehicle control but this is not maintained (Figure 2G), likely due to adaptive resistance of the tumor to continued targeted therapy.

We further profiled the on-target binding of our LSD1 inhibitor suite through assessment of the H3K4me2 mark and by use of the cellular thermal shift assay (CETSA). Western blotting in DIPG IV and VI lines treated with LSD1 inhibitors showed increased expression of the H3K4me2 mark consistently by GSK LSD1 in both lines (Figure 3A). Using CETSA, we could determine if LSD1 is bound by various LSD1 inhibitors in DIPG and NHA cells by heating live cells under treatment with candidate compounds and interrogating the thermostability of the target protein via western blot (Figure 3B). It was observed that all catalytic LSD1 inhibitors could bind LSD1 in all cell types, while results were less consistent with the scaffolding LSD1 inhibitor compounds (Figure 3C). We hypothesized that the dose of SP-2509 and SP-2577 may be too low to thermostabilize LSD1, so we conducted dose response CETSAs with TCP as a positive control. We found a ~50% increase in binding in DIPG VI by raising doses of SP-2509, but no increase in binding above DMSO control with higher doses of SP-2577 in either DIPG cell type (Figure 3D). Given that we dosed up to 100 μM for the dose response CETSA, which is almost 10 times the IC_{50} of the scaffolding inhibitors in DIPG cells, either the CETSA assay cannot capture the protein complex-disruption properties of the scaffolding compounds or there exists off-target effects, of which there is published data for rationale of the latter.[24,25]

With sensitivity and on-target activity of LSD1 inhibition in DIPG established, we next treated cells with subcytotoxic doses of LSD1 inhibitors for 24 h and isolated RNA to measure expression of our immune gene signature. DIPG cells display a significant upregulation of the signature under treatment with irreversible catalytic LSD1 inhibitors but no significant changes when treated with reversible scaffolding LSD1 inhibitors SP-2509 and its clinical successor SP-2577 (Seclidemstat). This gene signature was also selective for DIPG, as the same treatment

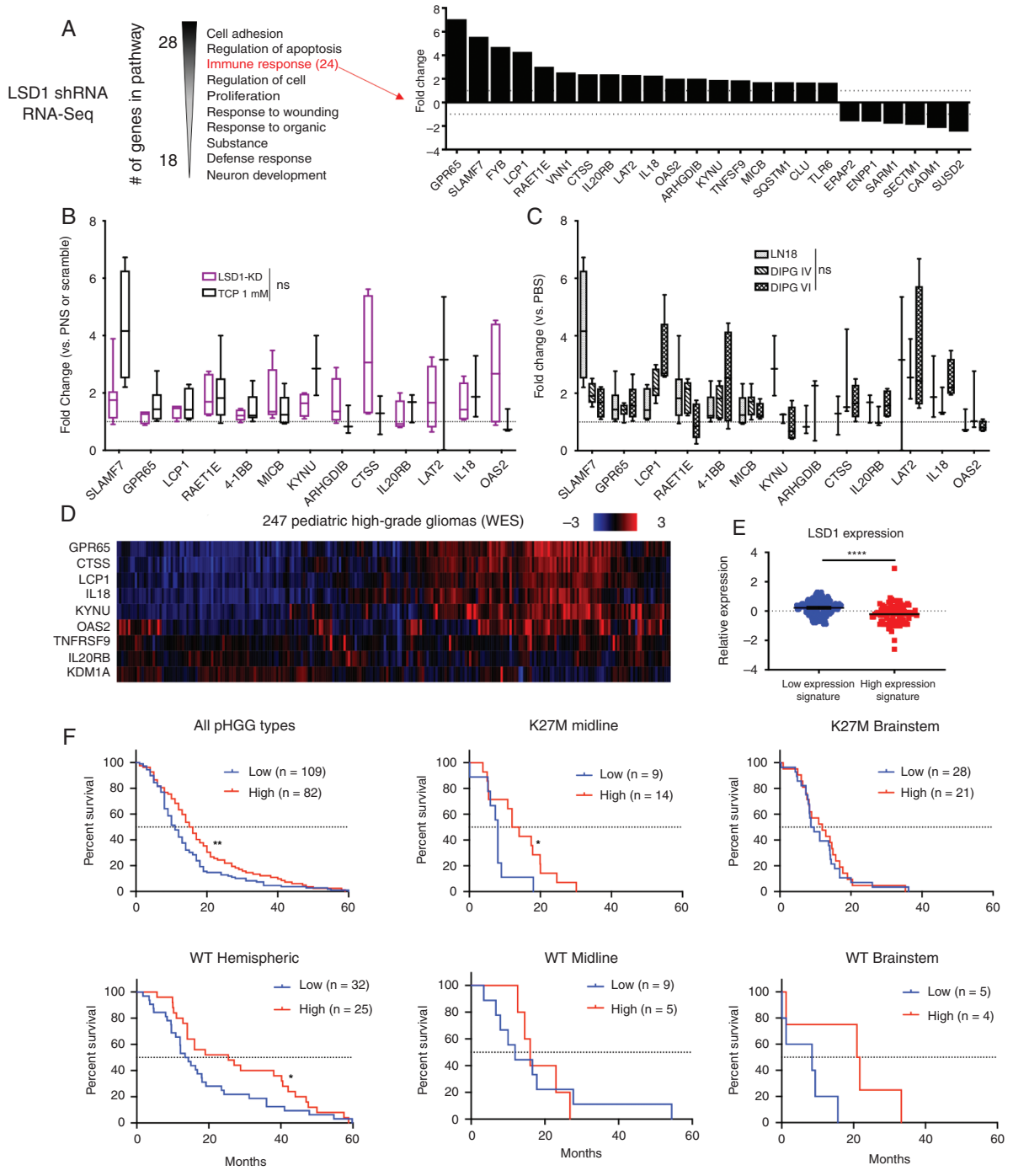

Fig. 1 LSD1 immunogenic signature is predictive of survival benefit in pediatric high-grade glioma patients. (A) RNA-Seq pathway analysis performed in LSD1 shRNA transduced LN18 cells. Immune response genes and associated fold changes are shown. (B) RT-qPCR of immune gene signature in LN18 cells with LSD1 shRNA or 1 mM TCP treatment for 24 h analyzed by one-way ANOVA with FDR correction. (C) RT-qPCR of immune gene signature in LN18, DIPG IV, and DIPG VI after 1 mM TCP treatment for 24 h analyzed by one-way ANOVA with FDR correction. (D) Heat map of pHGG patient exome data probed for LSD1 immune gene signature. (E) LSD1 expression of patients expressing high and low levels of gene signature analyzed by unpaired *t*-test. (F) Survival curves of pHGG patient data subdivided by histone mutation and tumor location and analyzed by log-rank or Wilcoxon tests. $^{*}P < 0.05$, $^{**}P < 0.01$, $^{****}P < 0.0001$, ns = not significant. At least 3 biological replicates were used for RT-qPCR experiments.

did not induce upregulation of NHA cells (Figure 4A, B). We confirmed this selectivity by using LSD1 siRNA in DIPG IV and NHA cells, where we observed upregulation in DIPG but not NHA, at comparable levels of LSD1 knockdown (Supplementary Material). Several genes in the signature correspond to immune signaling receptors, so we next

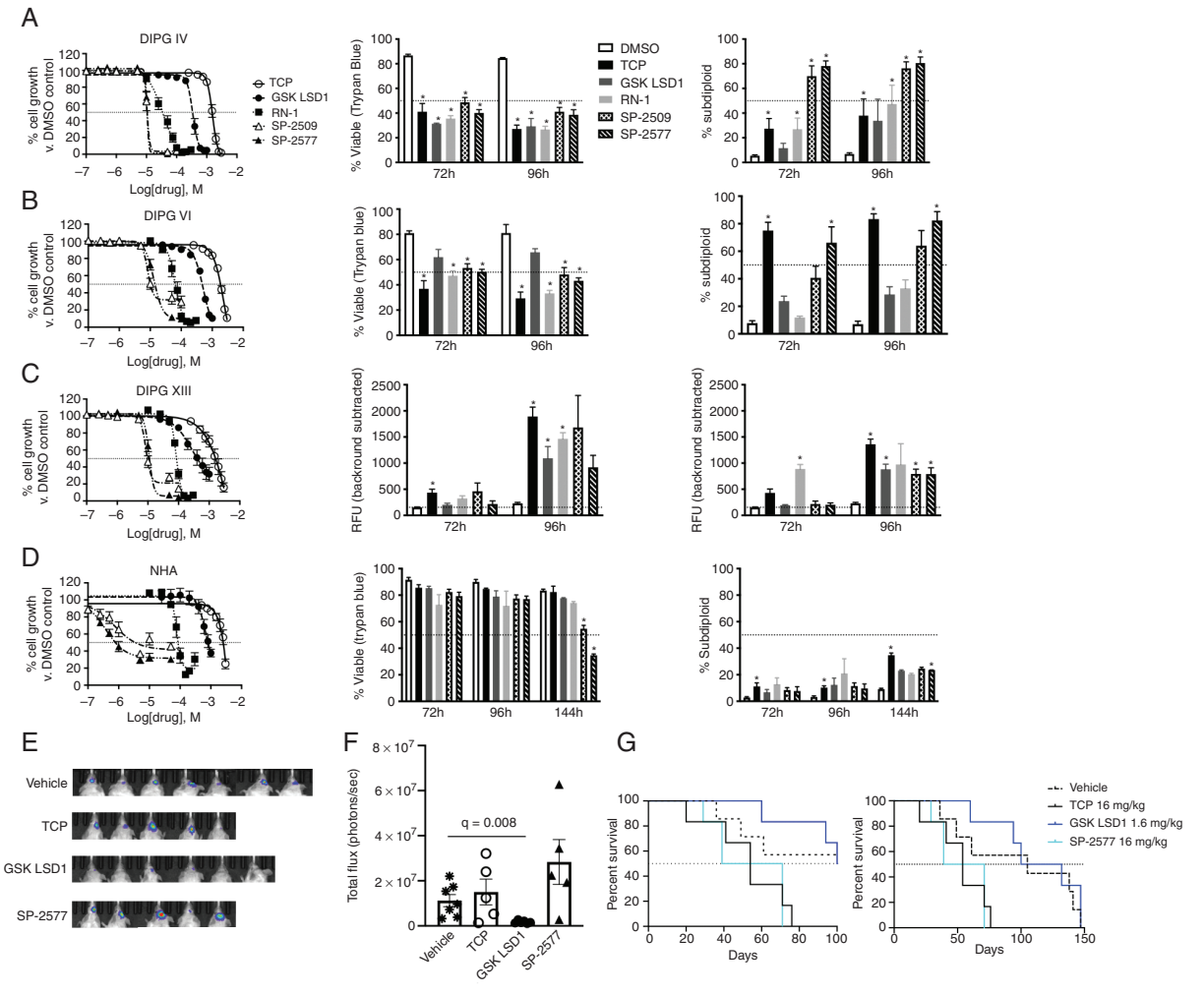

Fig. 2 LSD1 inhibitors are growth inhibitory in vitro and in vivo and induce selective cell death in DIPG cells. (A) Dose response curves of LSD1 inhibitors in DIPG IV, (B) DIPG VI, (C) DIPG XIII, and (D) NHA measured using alamarBlue after 120 h treatment. Cell viability after 72 and 96 h measured using trypan blue cell exclusion and analyzed by *t*-test comparing with DMSO control using FDR correction. DNA fragmentation measured using propidium iodide on flow cytometry analyzed by T-test comparing with DMSO control using false discovery rate (FDR) correction. Cell death of DIPG XIII (C) measured using GelGreen fluorescent intensity in 96-well plate reader and analyzed by *t*-test comparing with DMSO control using FDR correction. (E) Images of orthotopic tumor luminescence in an NSG pHGG hemispheric mouse model. Mice are shown after 2 weeks of treatment and 4 weeks after tumor implantation. (F) Quantification of tumor burden shown in (E). Vehicle group compared with GSK LSD1 group via *t*-test with FDR correction. (G) Survival curves of NSG pHGG mice at 100 days and 150 days. $*P < 0.05$. At least 3 biological replicates were used for all experiments. Error bars represent mean ± SEM.

profiled protein expression of 3 innate immune receptors known to play roles in NK cell signaling (SLAMF7, MICB, and ULBP-4). Using flow cytometry, we found that DIPG cells display differing baseline levels of these receptors, perhaps due to their mutational differences in histone alleles (H3.1 versus H3.3). Overall, however, we could detect increased expression on live cells after LSD1 inhibitor treatment for 48 h (Figure 4C).

The above receptors function either as ligands of natural killer group 2 member D (NKG2D) or as self-ligating receptors, and stimulation through these receptors increases NK cell activity and lysis of target cells. Given our observed upregulation of these receptors under LSD1 inhibition, we hypothesized that NK cells would lyse target DIPG cells more readily upon LSD1 inhibition. Fluorescently labeled DIPG IV and VI cells were incubated with effector human NK cells at various effector to target (E:T) ratios. Across 3 unique healthy blood donors from whom we expanded NK cells, we could observe increases in lysis in 2 DIPG lines when treated with catalytic LSD1 inhibitors TCP and GSK LSD1, but inconsistently under scaffolding LSD1 inhibition by SP-2509 (Figure 5A). We hypothesize discrepancies between DIPG IV and VI to be due to higher basal levels of ULBP-4 in DIPG VI and greater upregulation of ULBP-4 in DIPG VI after pre-treatment with SP-2509 (Figure 4C). Notably, the lysis efficacy of expanded healthy human donor T cells was much lower than NK cells, and could not be augmented by LSD1 inhibitor pretreatment (Figure 5B).

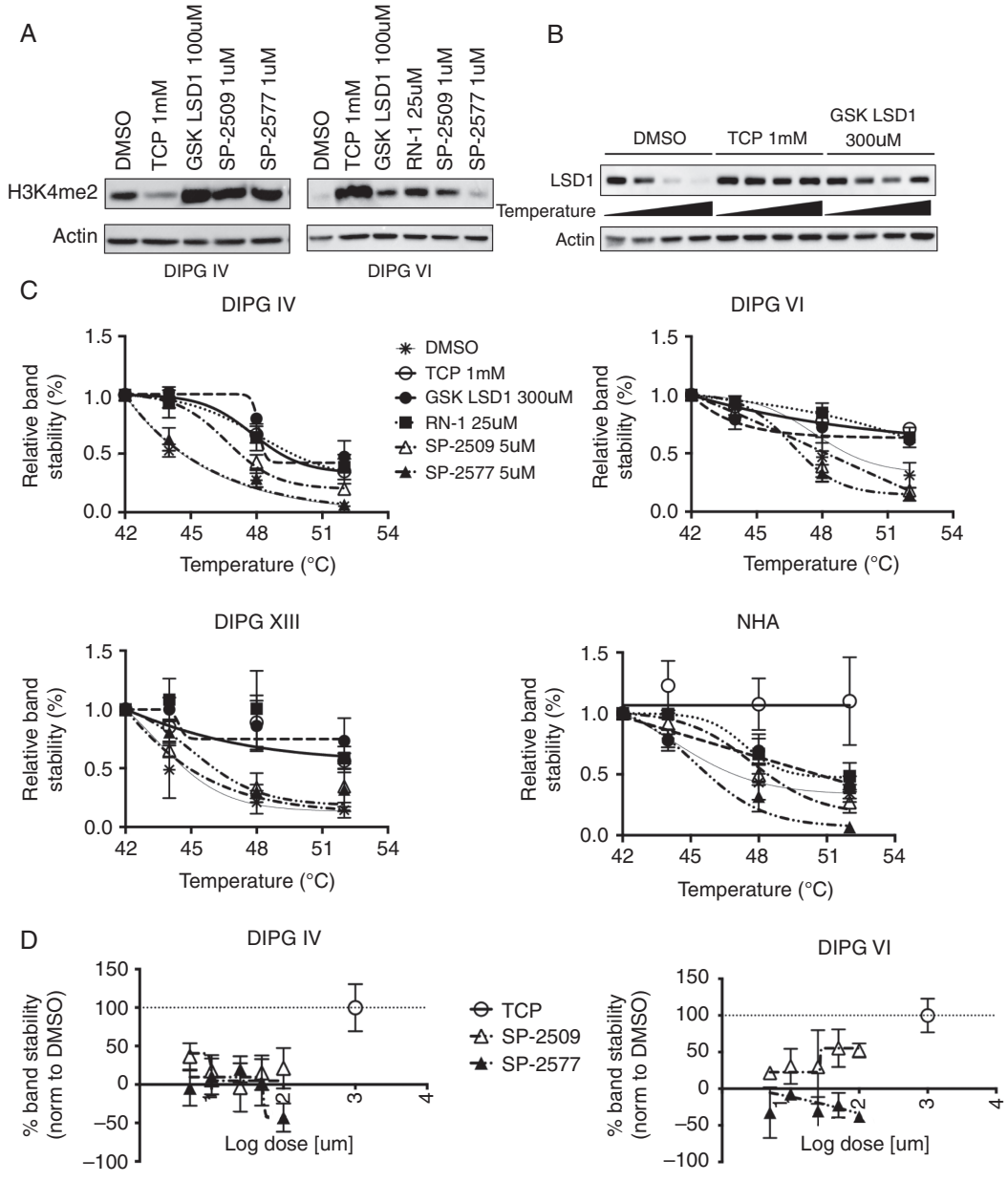

Fig. 3 LSD1 inhibitors alter histone methylation levels and thermostabilize LSD1 in DIPG and NHA cells. (A) Western blots of DIPG IV and VI cells treated with LSD1 inhibitors for 24 h and probed for H3K4me2 expression. (B) Representative western blot of CETSA probing LSD1 thermostability in DIPG VI cells. (C) Protein melt curves for LSD1 in different cell types. Each data point was normalized to beta-actin level and further normalized to 42°C data point for each experimental condition. (D) Dose response CETSA for scaffolding inhibitors SP-2509/2577. LSD1 was destabilized at 48°C for all doses and DMSO control was set as 0% stability and 1mM TCP was set as 100% stability. At least 3 biological replicates were used for all experiments. Error bars represent mean ± SEM.

We aimed to correlate genetic biomarkers of NK lysis by probing our gene signature from matched co-culture samples, and observed strong positive trends for 4 genes in DIPG IV (Figure 5C) and 2 genes in DIPG VI (Figure 5D). Unexpectedly, a negative correlation could be found for 4–1BB (Figure 5E), traditionally a T-cell stimulatory factor, which could indicate alternative function during NK cell engagement. Mice implanted with PKC-HA cells in the brainstem of syngeneic C57BL/6 mice and treated with catalytic LSD1 inhibitors (Figure 5F) showed increased expression of the gene signature in neural tissue harvested when mice were moribund (Figure 5G). Given that adaptive resistance to GSK LSD1 was seen in our mouse model (Figure 2G), we combined GSK LSD1 with NK cell infusion to model enhancement of innate immunity after LSD1 inhibition in vivo. Mice treated with intraperitoneal GSK LSD1 and intracranial human ex vivo expanded NK cells had the greatest reduction (43%) in tumor burden from baseline compared

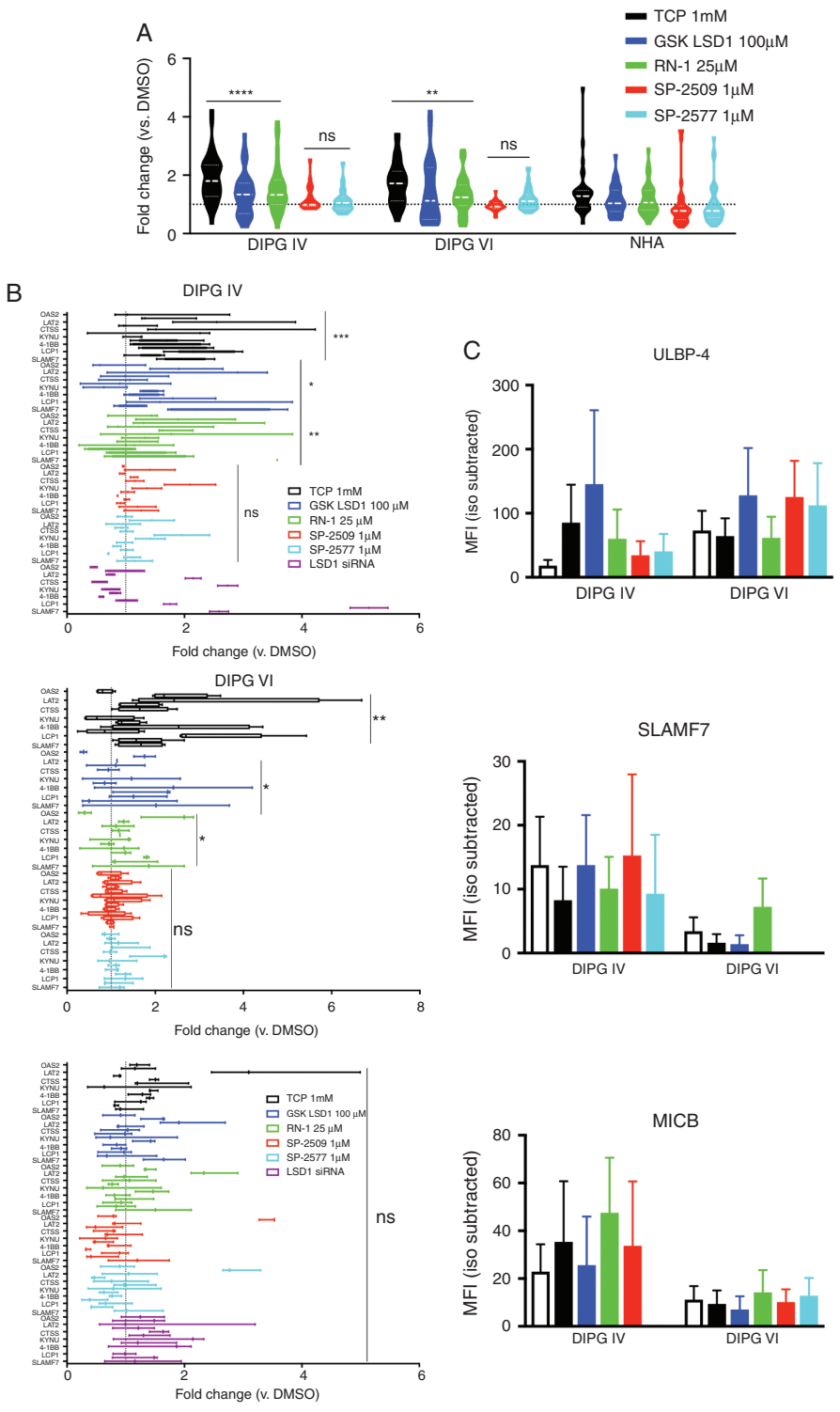

Fig. 4 Irreversible catalytic LSD1 inhibitors selectively generate immunogenic signature in DIPG cells. (A) RT-qPCR for immune gene signature performed on cells after treatment with indicated LSD1 inhibitors for 24 h. Catalytic inhibitors (TCP, GSK LSD1, and RN-1) and scaffolding inhibitors (SP-2509/2577) are compared with matched NHA controls using one-way ANOVA with FDR correction. (B) RT-qPCR data replotted with individual genes and including siRNA treatment for 48 h. Fold change compared with DMSO control analyzed via one-way ANOVA with FDR correction. (C) Median fluorescent intensity of indicated receptors after 48 h of LSD1 inhibitor treatment. Matched species and fluorophore isotype controls used to measure background fluorescence. (D) RT-qPCR data with individual genes from PKC-HA and PHC-HA murine cells. Fold change compared with DMSO control analyzed via one-way ANOVA with FDR correction. *$P < 0.05$, **$P < 0.01$, ***$P < 0.001$, ****$P < 0.0001$, ns = not significant. At least 3 biological replicates were used for all experiments. Error bars represent mean ± SEM.

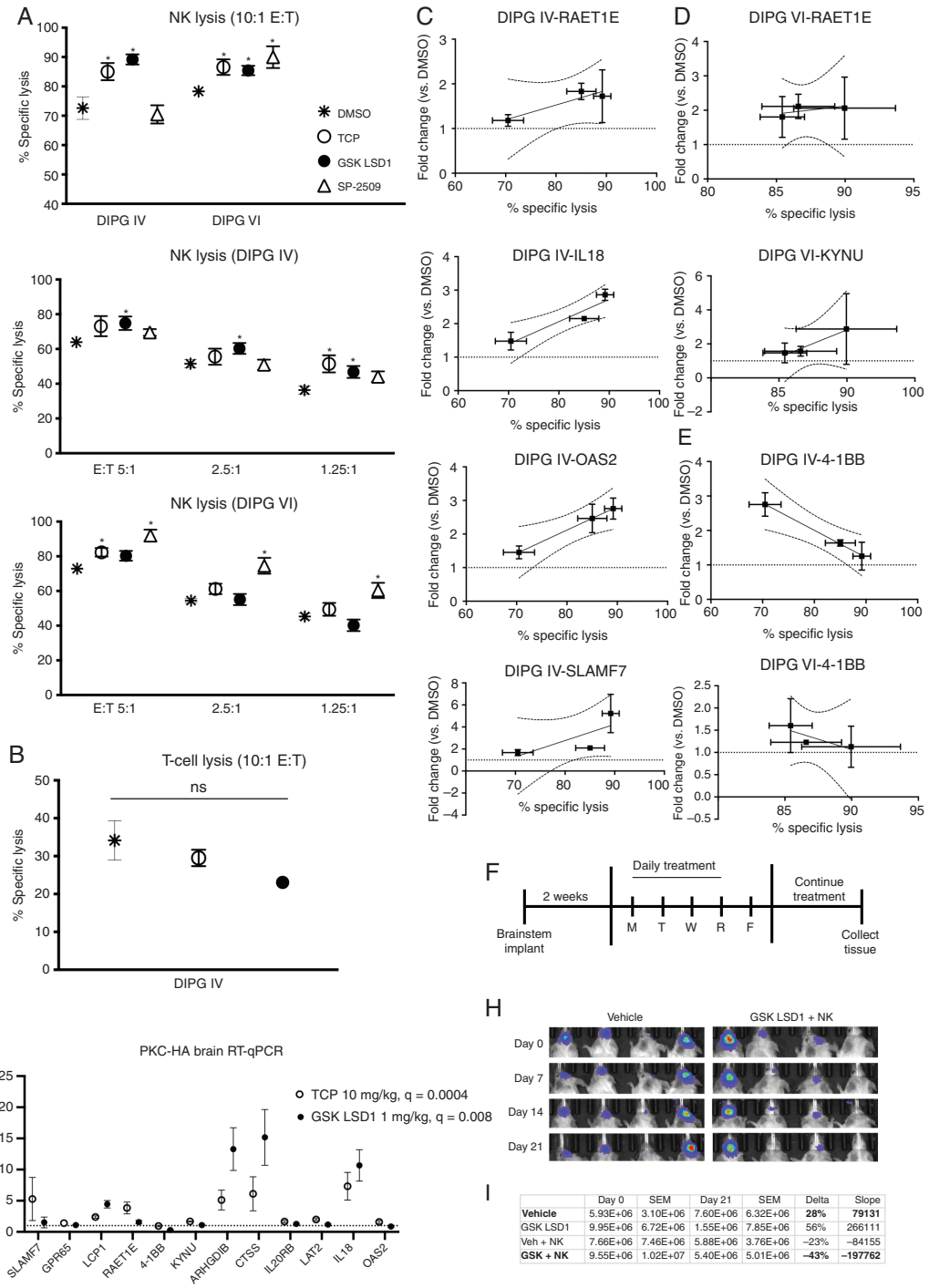

Fig. 5 LSD1 inhibition upregulates innate immune receptors and sensitizes DIPG cells to NK cell lysis which correlates with unique genetic identifiers of response. (A) Lysis of target DIPG cells co-cultured with NK cells after 48 h pretreatment of target cells with LSD1 inhibitors (TCP 0.5 mM, GSK LSD1 300 μM, SP-2509 5 μM). Treatments analyzed versus DMSO control using *t*-test with FDR correction. (B) Lysis of target DIPG cells co-cultured with T-cells after 48 h LSD1 inhibitor pretreatment. (C) DIPG IV RT-qPCR from matched co-culture experiments, genes with positive Pearson's correlation $R^2 > 0.80$ are shown with 95% CIs. (D) DIPG VI RT-qPCR from matched co-culture experiments. (E) RT-qPCR from matched co-culture experiments, negative correlation with $R^2 > 0.80$ shown with 95% CIs. (F) Schematic of immunocompetent C57BL/6 PKC-HA brainstem mouse model. (G) RT-qPCR was performed on RNA extracted from PKC-HA mouse brains. Fold change is plotted versus PBS control. TCP and GSK LSD1 were compared with PBS via one-way ANOVA with FDR correction. (H) Images of orthotopic tumor luminescence in NSG DIPG IV-luc mice starting from day 0 prior to start of treatment. (I) Tumor burden of NSG DIPG IV-luc mice quantified (photons/sec/cm^2) and analyzed for % change (delta) and linear regression (slope) between day 0 and day 21. $^*P < 0.05$ and ns = not significant. At least 3 biological replicates were used for all experiments. Error bars represent mean ± SEM.

with vehicle control, GSK LSD1 alone, or NK cells alone (Figures 5H, I). GSK LSD1 alone did not exert single agent anti-tumor efficacy in this human xenograft model, which is in contrast to our results in mouse orthotopic models, likely due to species mismatch. However, this highlights the anti-tumor effect of the combination of GSK LSD1 and NK cells as particularly striking.

To further validate our finding that catalytic LSD1 inhibition can enhance NK cell lysis of DIPG in vitro and in vivo, we revisited our patient data for analysis using CIBERSORT. We found that significant NK cell infiltration is positively prognostic for H3-WT hemispheric tumors, but CD8 T-cell infiltrate is negatively prognostic. Brainstem tumors benefited less from NK infiltrate, but significant NK presence was still a superior prognostic indicator versus CD8 T cells in the brainstem (Figure 6A). We next investigated how already-present or ex vivo infused immune cells would respond to LSD1 inhibition, and treated expanded NK and T cells with a panel of chromatin-modifier inhibitors including our LSD1 suite. As has been known,[26] T-cells are sensitive to HDAC inhibition, but are fairly resistant to LSD1 inhibition except at higher doses of the scaffolding inhibitors. Conversely, NK cells are resistant to HDAC inhibition but highly sensitive to scaffolding LSD1 inhibitors, with no live cells detected even at 500 nM doses of SP-2509/2577 (Figure 6B). Catalytic LSD1 inhibitors are comparatively nonperturbing, with the IC50s against NK cells being 2–10X higher than doses needed to induce our gene signature. Given our data showing the scaffolding LSD1 inhibitors are cytostatic but not cytotoxic to NHA cells, we profiled the metabolism of both NK and T-cells after LSD1 inhibitor treatment, as active metabolism of nutrients has been shown to be crucial to anti-tumor effects of both cell types. Strikingly, the scaffolding LSD1 inhibitors completely suppress the metabolism of NK cells, rendering them metabolically quiescent but still alive at 48 h posttreatment (Figure 6C). Collectively, these data suggest that catalytic LSD1 inhibitors may be used at therapeutic doses to induce increased NK cell reactivity without harming the NK cells directly.

Discussion

Here we have described a novel dual role for the histone demethylase LSD1 in controlling cell death and innate immune responses against pHGG and DIPG cells in vitro and in vivo. Expression of immune response genes accurately categorized pHGG patients' survival probability, and therapy with catalytic LSD1 inhibitors triggered gene expression changes that enhanced NK cell-mediated lysis. Epigenetic drugs targeting chromatin modifiers or readers have shown promising antitumor effects in preclinical DIPG models, but these agents have not yet been combined with clinically relevant immunotherapy regimens. NK cell administration is effective against malignant gliomas,[27] can be grown without autologous sources of leukocytes,[28] and has already begun clinical trials using our exact NK-expansion methodology,[29] including in pediatric solid tumors and brain tumors (NCT02271711, NCT03420963). Furthermore, combination therapy with LSD1 inhibitors is desirable due to the demonstrated selectivity of LSD1 inhibitor–induced DIPG cell death versus normal astrocytes. These results suggest the clinical potential of a regimen combining irreversible catalytic LSD1 inhibitors and NK cell infusion in pHGG.

LSD1 recently was shown to control the double-stranded RNA stress response and subsequently synergize with anti–programmed cell death 1 therapy in murine models.[30,31] Notably, this phenomenon was described only in epithelial-derived tissue such as breast, skin, and lung cancer cell lines. We could not recapitulate these genetic changes in our LSD1 shRNA RNA-Seq and believe this aspect of LSD1 influence on tumor immunity may be restricted to only certain cell types. Furthermore, these investigations did not thoroughly explore use of LSD1 inhibitors with differential mechanisms of action to induce enhanced adaptive immunity. DIPG and its microenvironment has recently been described as "immune cold" to the adaptive immune system but potentially vulnerable to modulation of innate immunity.[32–34] Another consideration is the pharmacokinetic (PK) properties of currently available LSD1 inhibitors, which have recently been shown to be ineffective against intracranial medulloblastoma despite very potent in vitro activity.[35] Our data indicate GSK LSD1 can cross the blood–brain barrier in hemispheric pHGG mouse models, suggesting intracranial tumor location plays a major role in the efficacy of GSK LSD1 against brain tumors. Two separate groups in Japan recently described new catalytic LSD1 inhibitors with favorable PK properties for potential use in neuro-oncology.[36,37] The transcription factor GFI1B is not disrupted by their compounds, reducing peripheral toxicity and sparing immune cells that would be critical for our combination therapy. Furthermore, they target the LSD1 catalytic site and may be able to induce the NK-boosting gene changes seen in our experiments.

NK cells have been shown to specifically target glioblastoma stem cells[38] and can circumvent antigen loss seen with chimeric antigen receptor T cell–based modalities.[39] A clinical trial of NK cell locoregional infusion for pediatric patients with posterior fossa malignant tumors is already in progress[40] and preliminary results indicate an excellent safety profile and feasibility of NK cell harvest and expansion. Our analyses of pHGG datasets indicating that a survival advantage is associated with hemispheric and midline tumors, but not brainstem tumors, that display the LSD1 gene signature and the CIBERSORT results of NK infiltrate suggests there are differences in vascularity between these tumor sites, which has been confirmed recently by another group.[41] Other promising clinically actionable drug candidates in DIPG could also be combined with NK cell therapy, such as the dopamine receptor D2–antagonist ONC201, which has been shown to recruit NK cells into tumors[42] and is currently in clinical trials in K27M+ tumors.[43] Oncolytic viruses targeting DIPG have also begun clinical trials,[44] and NK cells have been shown to be involved in the immune response to lysed tumor cells in the brain.[45] We did not yet test synergy of NK cells with standard-of-care radiotherapy or chemotherapy in our models, which is warranted based on preclinical[46,47] and clinical trial[48] data of adult gliomas.

The novel findings in our paper set the stage for further investigations into innate immune interactions in DIPG and how they can be therapeutically exploited with LSD1

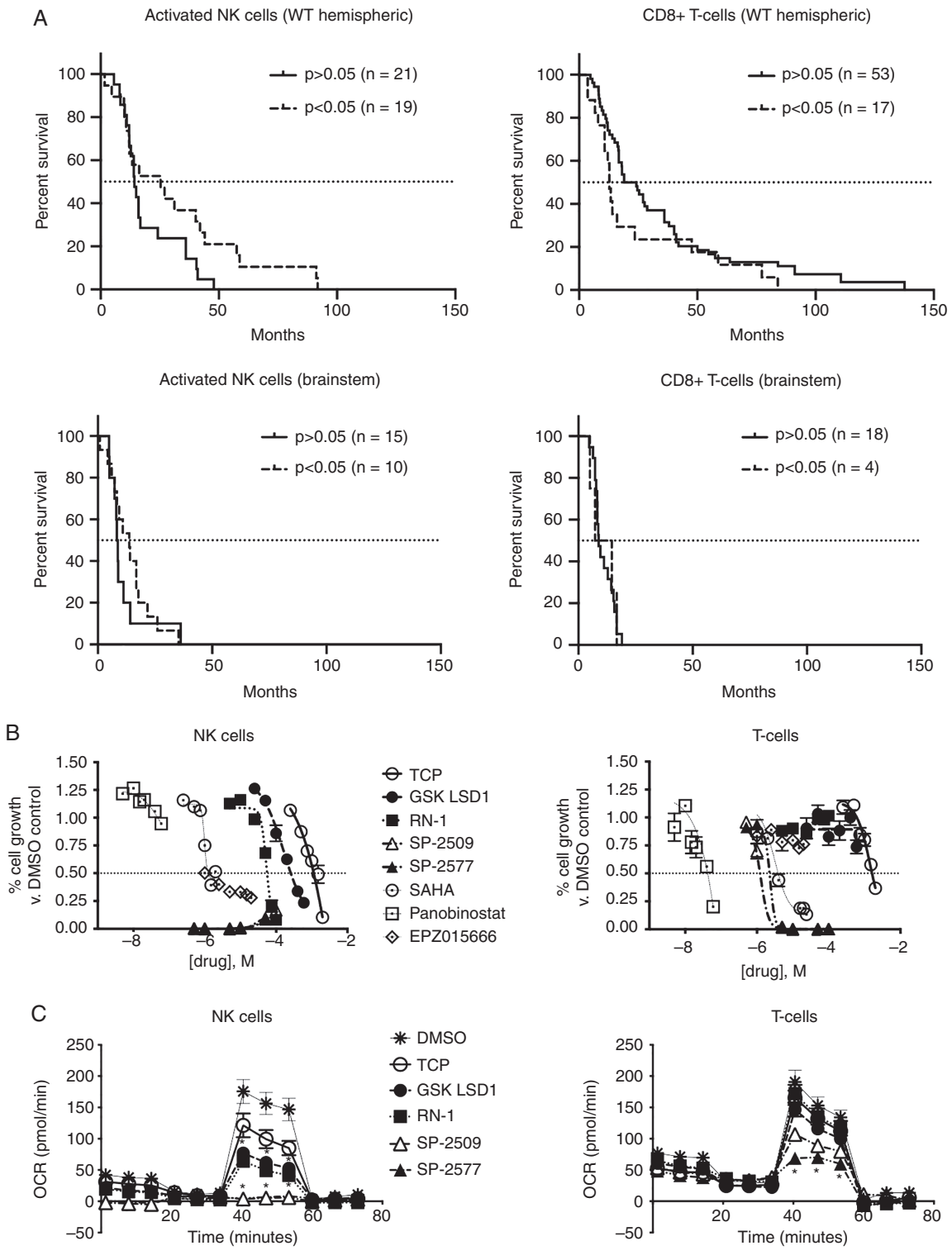

Fig. 6 NK cell tumor infiltration is predictive of survival benefit in pediatric high-grade glioma patients and catalytic LSD1 inhibitors are non-perturbing to mature NK and T cells. (A) CIBERSORT analysis of pHGG patient data sub-analyzed by tumor location and immune cell type. Survival curves show significant versus nonsignificant presence of indicated immune cell in patient tissue. (B) Purified expanding T and NK cells treated with indicated chromatin-modifier inhibitors for 120 h and measured using alamarBlue. (C) XF Mito Stress Test performed on NK and T cells after 48 h of LSD1 inhibitor treatment (TCP 0.5 mM, GSK LSD1 300 μM, RN-1 25 μM, SP-2509/2577 5 μM) and treatments compared with DMSO control analyzed by *t*-test with FDR correction. $^*P < 0.05$. At least 3 biological replicates or unique donors were used for all experiments. Error bars represent mean ± SEM.

inhibitors that can induce both cell death and NK cell reactivity in vitro and in vivo. Our extensive use of LSD1 inhibitors with unique binding properties suggests future investigation of combining brain-penetrant catalytic LSD1 inhibitors and NK cell infusions for synergistic killing of DIPG tumor tissue.

Supplementary Material

Supplementary data are available at *Neuro-Oncology* online.

Keywords

DIPG | epigenetics | immunotherapy | LSD1 | NK cell

Funding

This work was supported by the NIH under award numbers (i) R21 NS093387 (to J.C.); (ii) Brain Tumor SPORE P50 CA127001 (Developmental Research Project to JC); and (iii) P30CA016672 for use of the Characterized Cell Line Core and Research Animal Support Facility. We are also grateful for support from the Cancer Prevention Research Institute of Texas (CPRIT) grant RP150301 (to VG) and core facility grant RP170628, Center for Cancer Epigenetics at MD Anderson (Pilot Project Grant & Sequencing Core Allowance (to JC) and Scholar Award (to CPB)), and to the Schissler Family Foundation Fellowship (to CPB). Funding from the Team Connor Foundation; the Marnie Rose Foundation; and the Thomas Scott Family Foundation (to JC) is also gratefully acknowledged.

Acknowledgments

The authors thank Drs Michael Curran, Candelaria Gomez-Manzano, Andrew Gladden, and Min Gyu Lee for their input on experimental design and directions of the study. We thank Drs Ryan G. Kruger and Helai P. Mohammed for experimental suggestions; Drs Ruolan Han, Aundrietta Duncan, and Jeffrey L. Larson for providing SP-2577 and helpful discussions; Amanda C. Young and Jimi Lynn Young for preparation of tissue slides and IHC; Dr Collene R. Jeter and Jennifer J. Terpstra for immunofluorescence staining and imaging; and Dr Xiaoping Su and Clark Andersen for consultations on biostatistics and bioinformatics analysis.

Conflict of interest statement. The authors declare no relevant conflicts of interest.

Authorship statement. Generated hypotheses, performed experimental procedures, designed experiments, interpreted data and wrote manuscript: C.P.B., M.F., A.G., B.A.K., T.C., V.H., L.W., J.N., W.Z., J.C. Generated and provided cells and designed experiments: Y.Y., M.M.R., O.J.B., M.M., S.Y., D.A.L., V.G.

References

1. Johung TB, Monje M. Diffuse intrinsic pontine glioma: new pathophysiological insights and emerging therapeutic targets. *Curr Neuropharmacol*. 2017;15(1):88–97.
2. Wang SS, Bandopadhayay P, Jenkins MR. Towards immunotherapy for pediatric brain tumors. *Trends Immunol*. 2019;40(8):748–761.
3. Schwartzentruber J, Korshunov A, Liu XY, et al. Driver mutations in histone H3.3 and chromatin remodelling genes in paediatric glioblastoma. *Nature*. 2012;482(7384):226–231.
4. Lewis PW, Müller MM, Koletsky MS, et al. Inhibition of PRC2 activity by a gain-of-function H3 mutation found in pediatric glioblastoma. *Science*. 2013;340(6134):857–861.
5. Louis DN, Perry A, Reifenberger G, et al. The 2016 World health organization classification of tumors of the central nervous system: a summary. *Acta Neuropathol*. 2016;131(6):803–820.
6. Grasso CS, Tang Y, Truffaux N, et al. Functionally defined therapeutic targets in diffuse intrinsic pontine glioma. *Nat Med*. 2015;21(6):555–559.
7. Hashizume R, Andor N, Ihara Y, et al. Pharmacologic inhibition of histone demethylation as a therapy for pediatric brainstem glioma. *Nat Med*. 2014;20(12):1394–1396.
8. Mohammad F, Weissmann S, Leblanc B, et al. EZH2 is a potential therapeutic target for H3K27M-mutant pediatric gliomas. *Nat Med*. 2017;23(4):483–492.
9. Piunti A, Hashizume R, Morgan MA, et al. Therapeutic targeting of polycomb and BET bromodomain proteins in diffuse intrinsic pontine gliomas. *Nat Med*. 2017;23(4):493–500.
10. Cooney T, Onar-Thomas A, Huang J, et al. Dipg-22. a phase 1 trial of the histone deacetylase inhibitor panobinostat in pediatric patients with recurrent or refractory diffuse intrinsic pontine glioma: a pediatric brain tumor consortium (Pbtc) study. *Neuro Oncol*. 2018;20(suppl_2):i53.
11. Fu X, Zhang P, Yu B. Advances toward LSD1 inhibitors for cancer therapy. *Future Med Chem*. 2017;9(11):1227–1242.
12. Maes T, Mascaro C, Tirapu I, et al. ORY-1001, a potent and selective covalent KDM1A inhibitor, for the treatment of acute leukemia. *Cancer Cell*. 2018;33(3):495–511.e412.
13. Sankar S, Theisen ER, Bearss J, et al. Reversible LSD1 inhibition interferes with global EWS/ETS transcriptional activity and impedes Ewing sarcoma tumor growth. *Clin Cancer Res*. 2014;20(17):4584–4597.
14. Gupta S, Doyle K, Mosbruger TL, et al. Reversible LSD1 inhibition with HCI-2509 induces the p53 gene expression signature and disrupts the MYCN signature in high-risk neuroblastoma cells. *Oncotarget*. 2018;9(11):9907–9924.
15. Cusan M, Cai SF, Mohammad HP, et al. LSD1 inhibition exerts its antileukemic effect by recommissioning PU.1- and C/EBPα-dependent enhancers in AML. *Blood*. 2018;131(15):1730–1742.
16. Mohammad HP, Smitheman KN, Kamat CD, et al. A DNA hypomethylation signature predicts antitumor activity of LSD1 inhibitors in SCLC. *Cancer Cell*. 2015;28(1):57–69.
17. Maiques-Diaz A, Spencer GJ, Lynch JT, et al. Enhancer activation by pharmacologic displacement of LSD1 from GFI1 induces differentiation in acute Myeloid Leukemia. *Cell Rep*. 2018;22(13):3641–3659.
18. Pishas KI, Lessnick SL. Ewing sarcoma resistance to SP-2509 is not mediated through KDM1A/LSD1 mutation. *Oncotarget*. 2018;9(92):36413–36429.

19. Singh MM, Manton CA, Bhat KP, et al. Inhibition of LSD1 sensitizes glioblastoma cells to histone deacetylase inhibitors. *Neuro Oncol.* 2011;13(8):894–903.
20. Singh MM, Johnson B, Venkatarayan A, et al. Preclinical activity of combined HDAC and KDM1A inhibition in glioblastoma. *Neuro Oncol.* 2015;17(11):1463–1473.
21. Mackay A, Burford A, Carvalho D, et al. Integrated molecular meta-analysis of 1,000 pediatric high-grade and diffuse intrinsic Pontine Glioma. *Cancer Cell.* 2017;32(4):520–537.e525.
22. Somanchi SS, Lee DA. Ex vivo expansion of human NK cells using K562 engineered to express membrane bound IL21. *Methods Mol Biol.* 2016;1441:175–193.
23. Newman AM, Liu CL, Green MR, et al. Robust enumeration of cell subsets from tissue expression profiles. *Nat Methods.* 2015;12(5):453–457.
24. Sonnemann J, Zimmermann M, Marx C, et al. LSD1 (KDM1A)-independent effects of the LSD1 inhibitor SP2509 in cancer cells. *Br J Haematol.* 2018;183(3):494–497.
25. Mascaró C, Ortega A, Carceller E, et al. Chemoprobe-based assays of histone lysine demethylase 1A target occupation enable in vivo pharmacokinetics and pharmacodynamics studies of KDM1A inhibitors. *J Biol Chem.* 2019;294(20):8311–8322.
26. Bensaid D, Blondy T, Deshayes S, et al. Assessment of new HDAC inhibitors for immunotherapy of malignant pleural mesothelioma. *Clin Epigenetics.* 2018;10:79.
27. Zhang C, Burger MC, Jennewein L, et al. ErbB2/HER2-specific NK cells for targeted therapy of glioblastoma. *J Natl Cancer Inst.* 2016;108(5):djv375.
28. Somanchi SS, Kennis BA, Gopalakrishnan V, Lee DA, Bankson JA. In vivo (19)F-magnetic resonance imaging of adoptively transferred nk cells. *Methods Mol Biol.* 2016;1441:317–332.
29. Ciurea SO, Schafer JR, Bassett R, et al. Phase 1 clinical trial using mbIL21 ex vivo-expanded donor-derived NK cells after haploidentical transplantation. *Blood.* 2017;130(16):1857–1868.
30. Sheng W, LaFleur MW, Nguyen TH, et al. LSD1 ablation stimulates anti-tumor immunity and enables checkpoint blockade. *Cell.* 2018;174(3):549–563.e519.
31. Qin Y, Vasilatos SN, Chen L, et al. Inhibition of histone lysine-specific demethylase 1 elicits breast tumor immunity and enhances antitumor efficacy of immune checkpoint blockade. *Oncogene.* 2019;38(3):390–405.
32. Lieberman NAP, DeGolier K, Kovar HM, et al. Characterization of the immune microenvironment of diffuse intrinsic pontine glioma: implications for development of immunotherapy. *Neuro Oncol.* 2019;21(1):83–94.
33. Haberthur K, Brennan K, Hoglund V, et al. NKG2D ligand expression in pediatric brain tumors. *Cancer Biol Ther.* 2016;17(12):1253–1265.
34. Mackay A, Burford A, Molinari V, et al. Molecular, pathological, radiological, and immune profiling of non-brainstem pediatric high-grade glioma from the HERBY phase II randomized trial. *Cancer Cell.* 2018;33(5):829–842.e825.
35. Lee C, Rudneva VA, Erkek S, et al. Lsd1 as a therapeutic target in Gfi1-activated medulloblastoma. *Nat Commun.* 2019;10(1):332.
36. Saito S, Kikuchi J, Koyama D, et al. Eradication of central nervous system leukemia of T-cell origin with a brain-permeable LSD1 inhibitor. *Clin Cancer Res.* 2019;25(5):1601–1611.
37. Matsuda S, Baba R, Oki H, et al. T-448, a specific inhibitor of LSD1 enzyme activity, improves learning function without causing thrombocytopenia in mice. *Neuropsychopharmacology.* 2019;44(8):1505–1512.
38. Haspels HN, Rahman MA, Joseph JV, Gras Navarro A, Chekenya M. Glioblastoma stem-like cells are more susceptible than differentiated cells to natural killer cell lysis mediated through killer immunoglobulin-like receptors-human leukocyte antigen ligand mismatch and activation receptor-ligand interactions. *Front Immunol.* 2018;9:1345.
39. O'Rourke DM, Nasrallah MP, Desai A, et al. A single dose of peripherally infused EGFRvIII-directed CAR T cells mediates antigen loss and induces adaptive resistance in patients with recurrent glioblastoma. *Sci Transl Med.* 2017;9(399):1–15.
40. Khatua S, Sandberg D, Ketonen L, et al. Ept-02phase I study of fourth ventricle infusions of autologous Ex-Vivo expanded Nk cells in children with recurrent/refractory malignant posterior fossa tumors of the central nervous system. *Neuro Oncol.* 2016;18(suppl_3):iii24.
41. Wei X, Hartley R, Bear H, Fuller C, Phoenix TN. Hgg-13. Determining regional differences in high-grade glioma vasculature phenotype. *Neuro Oncol.* 2019;21(Supplement_2):ii89.
42. Wagner J, Kline CL, Zhou L, et al. Dose intensification of TRAIL-inducing ONC201 inhibits metastasis and promotes intratumoral NK cell recruitment. *J Clin Invest.* 2018;128(6):2325–2338.
43. Chi AS, Tarapore RS, Hall MD, et al. Pediatric and adult H3 K27M-mutant diffuse midline glioma treated with the selective DRD2 antagonist ONC201. *J Neurooncol.* 2019;145(1):97–105.
44. Tejada S, Díez-Valle R, Domínguez PD, et al. DNX-2401, an oncolytic virus, for the treatment of newly diagnosed diffuse intrinsic pontine gliomas: a case report. *Front Oncol.* 2018;8:61.
45. Kim Y, Yoo JY, Lee TJ, et al. Complex role of NK cells in regulation of oncolytic virus-bortezomib therapy. *Proc Natl Acad Sci U S A.* 2018;115(19):4927–4932.
46. Weiss T, Weller M, Guckenberger M, Sentman CL, Roth P. NKG2D-based CAR T cells and radiotherapy exert synergistic efficacy in Glioblastoma. *Cancer Res.* 2018;78(4):1031–1043.
47. Suryadevara CM, Desai R, Abel ML, et al. Temozolomide lymphodepletion enhances CAR abundance and correlates with antitumor efficacy against established glioblastoma. *Oncoimmunology.* 2018;7(6):e1434464.
48. Pellegatta S, Eoli M, Cuccarini V, et al. Survival gain in glioblastoma patients treated with dendritic cell immunotherapy is associated with increased NK but not CD8+ T cell activation in the presence of adjuvant temozolomide. *Oncoimmunology.* 2018;7(4):e1412901.